Pan-African Charnockites in the Shillong-Meghalaya Gneissic Complex, Northeast India and its implications

Pritom Borah (pritomborah90@gmail.com)
Gauhati University
Amulya Chandra Mazumdar
Gauhati University
Balen Bhagabaty
Gauhati University
Medard Augustine Khonglah
Geological Survey of India
Abhijit Bardoloi
Cotton University
Abhijit Bhattacharya
Indian Institute of Technology Kharagpur

Research Article

Keywords: Charnockites, Shillong-Meghalaya Gneissic Complex, P-T pseudosection analysis, Whole rock chemistry, Monazite chemical dating

Posted Date: March 20th, 2023

DOI: https://doi.org/10.21203/rs.3.rs-2687605/v1

Additional Declarations: No competing interests reported.

Pan-African Charnockites in the Shillong-Meghalaya Gneissic Complex, Northeast India and its implications

Pritom Borah[1] • Amulya Chandra Mazumdar[1,2] • Balen Bhagabaty[1] • Medard Augustine Khonglah[3] • Abhijit Bardoloi[2] • Abhijit Bhattacharya[4]

✉ Pritom Borah

E-mail address of Corresponding author: pritomborah90@gmail.com

1 Department of Geological Sciences, Gauhati University, Guwahati 781 014, India

2 Department of Geology, Cotton University, Guwahati 781 001, India

3 Geological Survey of India, North Eastern Region, Shillong 793 006, India

4 180B, Hijli Co-operative Society, Kharagpur 721 306, India

Abstract

Metamorphic to magmatic ortho/clinopyroxene bearing, massive to foliated charnockites *sensu lato* are exposed in the central part of the Shillong-Meghalaya Gneissic Complex (SMGC), Northeast India. The two pyroxene bearing metamorphic (group-1) charnockites are tonalitic to granodioritic in composition and together with associated high grade rocks pre-date all deformational episodes and successive metamorphic events. On the contrary, the orthopyroxene bearing (group-2) and fayalite + quartz bearing (group-3) magmatic charnockites post-date all deformational and metamorphic episodes. Both group-2 and -3 charnockites are granitic in composition. Thermobarometric estimations and quantitative P-T pseudosection modeling constrain the peak metamorphism of Group-1 charnockites at 900°C/ 6–6.5 kbar indicating a clockwise P-T trajectory. The ferroan to magnesian charnockites are calc-alkalic to calcic, and weakly peraluminous/metaluminous. The A_2-type charnockites with strongly fractionated REE patterns [$(La/Lu)_N$: 3.95–27.87] and negative Eu anomalies (Eu/Eu*: 0.28–0.46) are depleted in Nb, Ta, Sr and Ti abundances that correspond with a post-collisional setting. By comparison, in the associated mafic granulites as enclaves/bands, the REEs are 10-60 times enriched relative to chondrite, have flat patterns, and with no negative Eu anomalies. The charnockite suite is derived by the partial melting of varied protoliths including garnet-bearing amphibolites and crustal sources. Tightly-constrained chemical dates in chemically-zoned monazites, hosted within recrystallized grains of pyroxenes and plagioclase in three charnockites samples vary between 463±40 and 526±37 Ma (mean: 503±4 Ma). The magmatic to metamorphic charnockites attest to the prevalence of high-T during the period of post-collisional East Gondwana assembly related accretion at a late stage of Pan-African orogenic cycle, arguably continuous with the Pan-African Prydz Bay suture (East Antarctica) within the East Gondwanaland.

Keywords Charnockites • Shillong-Meghalaya Gneissic Complex • P-T pseudosection analysis • Whole rock chemistry • Monazite chemical dating

Introduction

Frost and Frost (2008) consider “charnockites” to be felsic igneous rock, broadly granite-granodiorite in composition, containing magmatic orthopyroxene, and/or olivine + quartz.

However, it has also been suggested that Opx and/or Cpx bearing gneisses of metamorphic settings involving the breakdown of hornblende, biotite ± garnet as a result of dehydration reaction, can be termed as charnockite or charnockitic gneiss (Frost and Frost 2008; Touret and Huizenga 2012). Magmatic charnockites are "dry" magmas formed at high temperature (>950ºC; Tubosun et al. 1984; Kilpatrick and Ellis 1992; Nedelec et al. 2000) and reducing conditions, i.e. Δ log QFM ≈ 0 (Frost and Frost 2008). Fluid inclusion studies reveal that orthopyroxene might stable if participating fluid of varied felsic magma could buffer to low-aH_2O fluid (Newton 1992: Santosh and Omori 2008: Touret and Huizenga 2012). These charnockites exhibit wide variations in composition, but little unanimity exist regarding the nature of the parent rock from which the charnockites are produced (Frost and Frost 2008). The charnockites are deemed to be differentiates or formed by partial melting of tholeiitic magmas (Frost and Frost 2008), or are produced by partial melting of LILE-enriched fertile granulite protoliths (Kilpatrick and Ellis 1992). Available geochemical and geochronological data from high grade Southern Granulite Terrain and Eastern Ghats Mobile Belt of Indian Peninsula suggested that the geochemical characteristics of Mesoarchean−Proterozoic to Early Paleozoic (~3.0 to 0.5 Ga) charnockite magmatism changes with distinct orogenic cycles (Rajesh 2012 and reference therein). In the Shillong-Meghalaya Gneissic Complex (SMGC), Northeast India, first incidence of charnockitic rock was reported from Mikir Hills, Assam (Pascoe 1950); while hypersthene bearing grey biotite gneiss (Gogoi 1975), charnockites and anorthositic rocks associated with granite gneiss were reported from the central part of SMGC (Bidyananda and Deomurari 2007; Khonglah et al. 2008 and references therein). In this study, we document the Pan-African (Cambro-Ordovician) charnockites in the Shillong-Meghalaya Gneissic Complex, and the only incidence of such young charnockite emplacements in India outside the Southern Granulite Terrain and the Kerala Khondalite Belt in the southern tip of the Indian Peninsula (Choudhary et al. 1992; Miller et al. 1996; Praharaj et al. 2021 and references therein). The existence of magmatic to metamorphic charnockites in SMGC attests to the prevalence of anomalously high temperature thermal perturbation (cf. Nedelec et al. 2000) during the Pan-African-Brasiliano orogenic cycle (Chatterjee et al. 2007; 2011). The Pan-African orogenic belt is inferred to be continuous (Chatterjee et al. 2007; 2011) with the Prydz Bay Pan-African suture in the East Antarctica within the East Gondwanaland (Tingey 1981; Stüwe et al. 1989; Boger et al. 2001).

Geological Background

The Shillong Plateau in the NE of India is an E–W oriented oblong horst block elevated to about 600–1900 m above the Gangetic alluvial plain (Figure 1A). The plateau is bound by the dextral Dawki fault in the South, Yamuna lineament to the West, and the Brahmaputra lineament in the North (Figure 1B). The Shillong-Meghalaya Gneissic Complex (SMGC) comprises rocks occurring in the Shillong Plateau, the Mikir Hills (Karbi Anglong, Assam), and as inselberg in the Quaternary sediments of the western Brahmaputra basins (Evans 1964; Crawford 1974; Desikachar 1974) (Figure 1B). The SMGC Precambrian crystalline rocks comprise NNE-striking, steep-dipping, and multiple-deformed amphibolite-granulite facies Paleo/Neoproterozoic ortho- and paragneisses, derived partly from Neoarchean/ Paleoproterozoic protoliths (Nandy 2001; Bidyananda and Deomurari 2007; Yin et al. 2010; Majumdar and Dutta 2016; Kumar et al. 2017a; Borah et al. 2019; Doley et al. 2022), deformed diorite plutons of unknown age, and equigranular to blastoporphyritic Early Mesoproterozoic and Late Neoproterozoic to Cambrian granitoid plutons. In the western part of the SMGC (Garo-Goalpara domain) (Figure 1B), the dominant gneisses are para-gneisses comprising biotite gneiss with sillimanite, ±cordierite, ±garnet, Sillimanite-Garnet-

Cordierite-Biotite gneiss, calc-silicate gneiss, mafic granulite, para-amphibolite, granodiorite gneiss, granite gneiss, and diorite intrusives (Chatterjee et al. 2007; 2011). By contrast, anatectic metapelite, augen gneiss and granite gneisses locally interleaved with amphibolite to granulite facies metabasic rocks, granodiorite gneiss as well as calc-silicate granulites dominate the east-central parts of the SMGC (Gogoi 1963; Mazumdar 1976; Lal et al. 1978). The east-central part is marked by the common occurrences of Early Paleozoic granitoid intrusions (Kumar et al. 2017a; 2017b; Sadiq et al. 2017).

U-Th-Pb$_{total}$ chemical dating of monazite of the amphibolite–granulite facies metapelites reveal predominantly Paleo/Mesoproterozoic dates (1830–1600 Ma; Chatterjee et al. 2007; 2011; Chatterjee 2017) with poorly constrained Late-Mesoproterozoic to Early Neoproterozoic (1140–950 Ma), Mid-Neoproterozoic (820 ± 21 Ma) and Late Neoproterozoic/Early Cambrian (650–520 Ma) dates (Chatterjee et al. 2007; 2011) in the western SMGC. Late Cambrian (494 ± 6 Ma; Chatterjee et al. 2011) monazite chemical dates are widely prevalent in the east-central part of SMGC, along with poorly constrained dates (1571−1472 Ma and 1078−1034 Ma; Chatterjee et al. 2007; Dwivedi et al. 2020). ~820 Ma xenotime chemical dates (Borah et al. 2019) indicate that the effects of this Mid-Neoproterozoic event are more common than previously thought in the east-central SMGC. U-Pb (zircon) dating indicates that the A-type Mayong granite in the northeastern margin and South Khasi granitoids in the southern part of the SMGC were emplaced at 1687 ± 35 Ma (Doley et al. 2022) and 520 ± 10 Ma (Kumar et al. 2017b), respectively. U–Pb zircon geochronology (Kumar et al. 2017a) yields Neoarchean to Paleoproterozoic dates (2566 ± 27, 1758 ± 54 and 1617 ± 14 Ma) for inherited zircon cores in the basement gneisses, implying thereby the involvement of recycled older crust in the generation of the Cambrian granites in the east-central SMGC. Three sets of concordant ages (1600, 1100 and 500 Ma; Yin et al. 2010) were obtained from U–Pb zircon dating in granite gneisses, granites and the Shillong

Group. Although, Bidyananda and Deomurari (2007) obtained zircon Pb-Pb ages (1077−1284 Ma) in a few charnockite samples from the Shillong Plateau, but the lack of geological setting, petrological and geochemical information on the samples limits the interpretation of such ages.

The Garo-Goalpara domain and the east-central Sonapahar-Nongstoin domain are deemed to have been welded during the Pan-African (Chatterjee et al. 2007; 2011; Chatterjee 2017). The Pan-African suturing is inferred based on the structural-metamorphic discord between the two domains, and the expansive occurrence of Cambro-Ordovician and Late Neoproterozoic granitoids within the east-central domain; however, the exact location of the zone of accretion is somewhat uncertain (Chatterjee et al. 2007; Borah et al. 2019). In this study, we investigate the existence of metamorphic to magmatic charnockite bodies associated with mafic granulites and granite gneiss in the Nongstoin-Markasa-Rambrai area (Figure 1B & C), in the east-central domain of the Shillong Plateau which were reported earlier (e.g. Pascoe 1950; Gogoi 1975; Bidyananda and Deomurari 2007; Khonglah et al. 2008). We provide the field settings, the metamorphic P-T evolutionary history, the whole rock geochemistry and monazite chemical ages in the charnockites and associated rocks.

Field Relations

The stocks and bosses of charnockites *sensu lato* in the Nongstoin-Markasa sector (Figure 1C) are inequigranular, coarse-grained and massive (Figure 2a), and of foliated varieties (Figure 2b). The massive charnockites contain irregular enclaves of mafic granulites (Figure 2c, f); the foliated varieties are interleaved with bands of mafic granulites, both sharing the same well-developed tectonic fabric (Figure 2b). In both the massive and foliated varieties, the contact between the mafic granulites and the charnockites are sharp. The charnockite bodies are wrapped by granite gneisses (Figure 2d). Patchy charnockite, similar to those reported by Pichamuthu (1960) in the Kabbaldurga quarry, are also observed locally (Figure 2e).

Petrography and Metamorphic Reactions

Charnockite *sensu lato*

On the basis of Quartz−K-feldspar−Plagioclase (Q-A-P) modal proportions, the orthopyroxene bearing charnockites *sensu lato* may be grouped as charnockite *sensu stricto* (granite in composition), charnoenderbite (granodiorite in composition) and enderbite (tonalite) following the classification of Streckeisen (1974; Figure 3). The constituent minerals are plagioclase (commonly antiperthite; X_{An} = 0.24–0.27), K-feldspar (dominantly mesoperthite; X_{Or} ~ 0.88), quartz, orthopyroxene (X_{Mg} = 0.34–0.36) with or without olivine, biotite and occasionally clinopyroxene (X_{An} = 0.24–0.27). The retrograde biotite and hornblende replace pyroxenes. The common accessories are apatite, magnetite, ilmenite, zircon, monazite and allanite. The mineral chemical compositions of mineral phases for the rocks are provided in supplementary table S1.

Based on the mineral abundances (in order of decreasing abundance), the charnockites *sensu lato* are classified into three groups, i.e.

Group-1: Plagioclase + Quartz + K-feldspar + Clinopyroxene + Orthopyroxene + Biotite ± (Ilmenite/Magnetite ± Monazite ±Apatite ± Zircon ± secondary Biotite)

Group-2: K-feldspar + Quartz + Plagioclase + Orthopyroxene + Hornblende ± (Monazite ± Magnetite ± Zircon ± Apatite ± secondary Biotite)

Group-3: K-feldspar + Quartz + Plagioclase + Fayalite ± (Magnetite ± Zircon ± Apatite ± Allanite ± secondary Biotite ± secondary Hornblende ± secondary Quartz)

The Group-1 charnockites are characterized by a granoblastic to inter-lobate texture superposed on a barely discernible tectonic foliation defined by the crude alignment of xenoblastic grains of orthopyroxene (Figure 4a). By contrast, Group-2 and -3 varieties are blastoporphyitic charnockites in which igneous textures dominate. In Group-2 charnockites, orthopyroxene and primary hornblende are the dominant mafic minerals, but clinopyroxene is lacking; Fe-rich olivine (and quartz) occurs in Group-3 charnockites.

The Group-1 charnockites are dominantly tonalite, and few samples plot in the field for granodiorite (Figure 3). The peak metamorphic assemblage includes plagioclase (X_{An} = 0.24–0.27), K-feldspar (X_{Or} ~ 0.88), quartz, orthopyroxene (X_{Mg} = 0.34–0.36) and clinopyroxene (X_{Mg} = 0.45–0.48). In the group-1 charnockites, rare inclusions of biotite lined with ilmenite blebs occur along the rims of orthopyroxene; discrete grains of xenomorphic quartz occur within the orthopyroxene grains (Figure 4b & c). These orthopyroxene hosted biotite and quartz grain, not in contact, constitutes the earliest metamorphic assemblage M_1.

The inclusions of biotite + quartz (M_1) within orthopyroxene indicate prograde metamorphism in the charnockites that produced the recrystallized aggregates of the peak metamorphic assemblage (M_2) of orthopyroxene and feldspars (Figure 4d). Biotite (X_{Mg} = 0.38–0.41) grains along the margin of pyroxene grains (Figure 4d) constitute a hydrous phase retrograde after M_2 minerals. The textural features such as symplectitic intergrowths of biotite and quartz at the contact between orthopyroxene and K-feldspar (Figure 4e) provide further evidence of post-M_2 retrogression (M_3).

The Group-2 charnockites are granitic in composition (Figure 3). They exhibit relict igneous textures, e.g. (a) euhedral to subhedral grains of plagioclase (Figure 5a), (b) partly recrystallized mantles around plagioclase phenocrysts, and (c) pyroxene-plagioclase intergrowths (Figure 5b). The thin quartz films around orthopyroxene, euhedral zircon crystal hosted within antiperthite in plagioclase (Figure 5c; Touret and Huizenga 2012), and symplectitic intergrowth of biotite + quartz at the contact of orthopyroxene in the absence of K-feldspar (Figure 5d) may indicate the presence of a melt phase, and hence attest to an igneous origin for the rock. The Group-2 charnockites lack primary biotite inclusion within orthopyroxene, as in the Group-1 charnockites. All biotite grains as well as biotite + quartz intergrowths are restricted to the margins of igneous pyroxenes in the Group-2 charnockites; these biotite grains are inferred to be retrograde alterations (M_3) induced by the post-emplacement hydration in the charnockites.

Group-3 charnockites are texturally similar to the Group-2 variety, but instead of orthopyroxene, olivine (fayalite) is ubiquitous in the rock (Figure 5e). The fayalite grains are lined with blebs and films of quartz (Figure 5f). Hornblende + quartz symplectites at the contact between the Fe-rich olivine (X_{Fe} = 0.96-0.97) and plagioclase (X_{An}= 0.18–0.20) (Figure 5g) and, biotite (X_{Fe} = 0.49–0.67) + quartz between olivine and K-feldspar (X_{Or} ~ 0.88) (Figure 5h) are common in the Group-3 charnockites. These textures suggest post-emplacement stabilization of hydrous phases (M_3) at the expense of M_2 assemblages in the charnockites.

Mafic granulites

The mafic granulites are medium to coarse-grained, massive to banded rocks that comprise dynamically recrystallized mosaic of orthopyroxene, clinopyroxene, plagioclase, ilmenite and green-brown hornblende. The mafic granulite may be grouped as hornblende-pyroxene granulites (hornblende, plagioclase, orthopyroxene, clinopyroxene, ilmenite/ magnetite with accessory apatite), and pyroxene granulites (plagioclase, orthopyroxene, clinopyroxene, ilmenite/magnetite, with hornblende as minor mineral of <3 modal%, and quartz, apatite, K-feldspar and rutile as accessory minerals). The mafic granulites are characterized by a crudely developed gneissic foliation (Figure 5i) modified by annealing recrystallization among hornblende, pyroxenes and feldspars in a polygonized mosaic (Figure 5j). Exsolved granules of ilmenite along the borders/fractures/cleavages of hornblende are common features in the hornblende-pyroxene granulites (Figure 5i). Also, exsolved K-feldspar grains along the margins of anti-perthites (Figure 5j) are common.

Summarizing, the inclusions of discrete grains of biotite and quartz (Figure 4b & c) hosted within orthopyroxene is possibly the only possible evidence that suggests prograde stabilization of the peak metamorphic assemblage (M_2) of the rocks vide the reaction,

Biotite + 3 Quartz = K-feldspar + 3 Orthopyroxene + H_2O (1)

However, the coexistence of the two-pyroxene + plagioclase + K-feldspar assemblages in the Group-1 charnockites may be attributed to the model prograde reaction (Mueller and Sexana 1977).

Biotite + Hornblende + 3 Quartz =

6 Orthopyroxene + Clinopyroxene + K-feldspar + Plagioclase + 2 H_2O (2)

In the mafic granulites, the prograde metamorphism from M_1 to M_2 is manifested by the rare occurrence of quartz and hornblende (never at the contact with each other) within orthopyroxene (Figure 5k). The concentration of ilmenite granules along the border of the green-brown hornblende (Figure 5i) in mafic granulites (Sen and Ray 1971a), and the negative correlation of modal amounts of hornblende vis-à-vis pyroxenes + plagioclase indicate that the stabilization of the M_2 granulite facies assemblage vide the model reaction.

Hornblende ± Quartz

= Orthopyroxene + Clinopyroxene + Plagioclase + H_2O (3)

Further, the persistence of quartz in pyroxene granulites indicates a positive role of silica in the prograde movement of the hornblende breakdown reaction (Sen and Ray 1971b).

On the other hand, the biotite + quartz intergrowths (M_3) replacing orthopyroxene at the contact with K-feldspar (Figure 4e) provides the only compelling evidence for fluid-induced retrogression of the M_2 peak metamorphic assemblage via the reaction

K-feldspar + 3 Orthopyroxene + H_2O = Biotite + 3 Quartz (4)

Metamorphic P-T Conditions

Metamorphic P-T estimation in charnockites, mafic granulites and granite gneisses was carried out using conventional mineral thermo-barometry. All EMP analyses of each mineral are provided in supplementary table S1. For P-T estimation, the orthopyroxene-clinopyroxene thermometer (Wood and Banno 1973; Wells 1977) and the orthopyroxene-biotite thermometer (Wu et al. 1999) was used for charnockites. The Ti-in Biotite (Henry et al. 2005) and the hornblende-plagioclase (Blundy and Holland 1990) thermometers were applied to charnockites, granite gneisses and mafic granulites. Pressure estimates were made using Al-in Hornblende (Hammarstrom and Zen 1986; Hollister et al. 1987; Schmidt 1992) in the mafic granulites, Group-2, 3 charnockites and granite gneisses. The results are provided in table 2.

M_2 metamorphic stage

The temperatures estimated using the two-pyroxene thermometer of Wood and Banno (1973) are 825 ± 29ºC and 821 ± 27ºC for Group-1 charnockites and mafic granulite, respectively. The corresponding temperatures obtained from the thermometric formulation of Wells (1977) are higher, i.e. 893 ± 45ºC and 882 ± 42ºC. On the other hand, hornblende-plagioclase thermometry (Blundy and Holland 1990) yielded relatively lower temperature of 787 ± 22ºC in the mafic granulite (Table 2).

Due to the absence of garnet and/or primary hornblende in Group-2 charnockite, pressure could not be estimated for these rocks. In mafic granulite, the pressures estimated from the Al-in hornblende barometers are 5.58 ± 0.46 (Hammarstrom and Zen 1986), 5.88 ± 0.51 (Hollister et al. 1987) and 5.96 ± 0.44 kbar (Schmidt 1992) (Table 2). Based on experiments on amphibole phase equilibria, Anderson and Smith (1995) suggest that Al-in hornblende geobarometer works best for Fe/(Fe+Mg) ratios in hornblende <0.6. In our samples, the Fe/(Fe+Mg) values in hornblendes are > 0.6.

M_3 metamorphic stage

The mean temperatures obtained for charnockites using the orthopyroxene-biotite exchange thermometer (Wu et al. 1999) and Ti-in biotite thermometers (Henry et al. 2005) are 649 ± 24°C and 768 ± 13°C, respectively. However, temperatures estimated from Ti-in biotite thermometry for granite gneiss are lower (mean T values <530ºC) (Table 2), and are unrealistic for the syn-S_2, M_3 assemblage. The average pressures obtained from granite gneiss (syn-S_2, M_3 assemblage) using Al-in hornblende geobarometer are 5.41 ± 0.18, 5.70 ± 0.20 and 5.81 ± 0.16 kbar (Hammarstrom and Zen 1986; Hollister et al. 1987; Schmidt 1992, respectively; Table 2).

By contrast, the mean temperatures estimated using the hornblende-plagioclase thermometry in Group-2 charnockites (Sample: L3A in Table 2) and Group-3 charnockites (Sample: Mar 114A in Table 2) are 756 ± 11ºC and 771 ± 16ºC, respectively. Relative to the hornblende-plagioclase thermometer, Ti-in biotite thermometry yields lower value, 688 ± 9ºC (Henry et al. 2005). The pressures estimated from the Al-in hornblende barometers in Group-2 and Group-3 charnockites taken together are 5.41 ± 0.26 and 5.37 ± 0.36 kbar (Hammarstrom and Zen 1986), 5.70 ± 0.29 and 5.66 ± 0.40 kbar (Hollister et al. 1987) and 6.00 ± 0.27 and 5.71 ± 0.34 kbar (Schmidt 1992), respectively.

P-T pseudosection Modeling

A P-T pseudosection is constructed for estimating the P-T path along which the metamorphic charnockites evolved. Calculations were performed using the Perple_X computer program (Connolly 2005; Version 6.8.6; http://www.perpleX.ethz.ch/) with an updated version of the internally consistent data set of Holland and Powell (2011) (data set tc-ds 62). All T-M(O_2), T-M(H_2O) and P-T pseudosection calculations were made for the model system Na_2O–CaO–K_2O–FeO–MgO–Al_2O_3–SiO_2–H_2O–TiO_2–O_2 (NCKFMASHTO) for the metamorphic variety (Group-1) charnockite sample NGB-304. The activity-composition models used for the pseudosection computations are Opx (W) for orthopyroxene, Gt(W) for garnet, Bi(W) for biotite, Ilm(WPH) for ilmenite and melt(W) for melt (White et al. 2014), Omph(GHP) for clinopyroxene (Green et al. 2007), cAmph(DP) for clinoamphibole (Diener et al. 2007), feldspar for ternary feldspar (Fuhrman and Lindsley 1988) and Sp(WPC) for spinel (Whiteet al. 2002). Bulk rock compositions of the rocks were determined by X-ray fluorescence spectroscopy at CSIR-National Geophysical Research Laboratory, Hyderabad. The chemical composition of charnockites sample used for pseudosection calculation is presented in table

3. To account for magnetite in sample NGB-304, Fe_2O_3 is incorporated into the calculations. The sample contains P_2O_5 up to 0.15wt% (Table 3) specifying equivalent to ~ 0.5 modal percent of apatite. Since P_2O_5 is not considered in the system NCKFMASHTO, the amount of w(CaO) present in apatite equivalent to the w(P_2O_5) content was calculated based on the stoichiometry of apatite and deducted from the calculation. Therefore, the modified w(CaO) content adopted for pseudosection calculation is 3.07 wt%.

The calculated T–M(O_2), T–M(H_2O) and P-T pseudosections of the selected sample NGB-304 from the central SMGC are presented in fig. 6. In the T–M(O_2) diagram (Figure 6a), the mineral assemblage plagioclase, orthopyroxene, clinopyroxene, K-feldspar, quartz, ilmenite, magnetite and inferred melt represents probable peak metamorphic assemblage, which is stable at M(O_2) range of 0.35−1.00. Further, the computed X_{En} isopleth 0.34 and X_{An} isopleth 0.25, which represent the mineral compositions obtained from electron probe microanalyses, intersect at M(O_2) = 0.98 (O_2 = 0.39 mol%), thus constraining an appropriate O_2 content. The calculated O_2 of 0.39 mol% was then used for T–M(H_2O) and PT pseudosection calculations. Since charnockites are devoid of garnet, it is difficult to measure the temperature-pressure conditions of the charnockites using conventional mineral geothermo-barometers. The T–M(H_2O) diagram used to constrain the water content as well as T–M(O_2) diagram were constructed at a pressure of 7.0 kbar, which is based on the pressure estimates on the associated granulitic grade rocks (Chatterjee et al. 2011). The charnockite formation in high-grade metamorphic condition is usually dry (e.g. Frost and Frost 2008; Rajesh and Santosh 2012), the isopleth intersection of orthopyroxene (X_{En}) and plagioclase (X_{An}) demarcates an appropriate water content of M(H_2O) = 0.22 (H_2O =1.01mol%; Figure 6b); this value was adopted for calculating the P-T pseudosection (Figure 6c). In the P-T pseudosection (Figure 6c), the solidus is confined within a temperature range of 810–863°C for pressures between 4 and 11 kbar. The assemblage biotite + orthopyroxene

+ plagioclase + K-feldspar + ilmenite + magnetite + quartz represent prograde metamorphic assemblage (Figure 4b & c). The lack of garnet in the charnockites suggest that the maximum pressure (<9.8 kbar) and temperature (<860°C) for the stability of the prograde metamorphic stage is constrained by the garnet-in line and the melt-in line, respectively (Figure 6c). The peak metamorphic assemblage plagioclase + orthopyroxene + clinopyroxene + quartz + K-feldspar + magnetite + ilmenite + inferred melt (Figure 4d) in the PT pseudosection is defined by the field bounded by garnet-in line, the presence of two-feldspar (plagioclase and K-feldspar) rather than one phase feldspar and Bt-out lines. The peak metamorphic assemblage shows a wide PT range of stability. The intersection of X_{En} =0.34 isopleth with X_{An}=0.25 isopleths at ~910°C and ~6.4 kbar constrains the PT condition of peak metamorphism (Figure 6c). The retrograde field is inferred by the ilmenite-out line at the upper pressure and melt-out line at the upper temperature with PT conditions of <820°C and <5 kbar. The assemblage orthopyroxene + clinopyroxene + biotite + plagioclase + K-feldspar + quartz + magnetite stable in the PT range of <745°C/<4 kbar to 820°C/5 kbar represents the retrograde metamorphism. This argument is supported by the formation of symplectitic intergrowth of biotite + quartz at the expense of orthopyroxene + K-feldspar (Figure 4e). From all results of PT pseudosection, it is inferred that the peak and retrograde temperature estimation likely conforms to the results of temperature of two pyroxene thermometry (~900°C; Well 1977) and Ti-in biotite thermometry (~770°C; Henry et al. 2005). In contrast, orthopyroxene-biotite thermometry (~649°C, Wu et al. 1999) shows lower temperature than Ti-in biotite most likely due to re equilibration of orthopyroxene and biotite. The possible prograde P-T path could not be constrained from the analyzed data.

Whole Rock Geochemistry

Whole rock major and trace elements data including the rare earth elements (REE) are presented in table 3. The charnockites (all quartz normative) have SiO_2 contents in the range 68.41−72.65 wt.%. The total alkalis (Na_2O+K_2O = 4.9–6.16 wt.%) and K_2O/Na_2O ratios (0.17–0.64) for Group-1 charnockites is lower than Group-2 (Na_2O+K_2O= 7.88−8.22 wt.%; K_2O/Na_2O= 1.67−1.76)and Group-3 charnockites and granite gneisses (Na_2O + K_2O= 7.15−7.60 wt.%; K_2O/Na_2O= 1.60−1.78). The mafic granulites (all olivine normative) are characterized by relatively low SiO_2-content (46.09−48.66 wt.%.), high MgO (8.99−10.15 wt.%), FeO (12.40−13.57 wt.%), and TiO_2 contents are in the range 1.00−2.10 wt.%; the total alkalis (Na_2O+K_2O) with K_2O/Na_2O ratios are lower, i.e. 3.39−3.93 wt.% and 0.38−0.52 respectively.

The Group-1 charnockites are magnesian and calcic type while Group- 2, 3 charnockites and granite gneisses are ferroan and alkali-calcic to calc-alkalic (Figure 7a, b). The FeO/MgO ratios in Group-2 (3.93−5.10) and Group-3 and the granite gneisses (7.28−13.27) are higher relative to the Group-1 charnockites (2.42−4.30). The Group-1 and the Group-2 charnockites are dominantly metaluminous, whereas the Group-3 charnockites and granite gneisses are peraluminous to weakly metaluminous (Figure 7c). Group-1 charnockites are characterized by low-K tholeiite to medium-K calc-alkaline series while Group-2, 3 charnockites and granite gneiss belong to high-K calc-alkaline series (Figure 7d). In contrast, the mafic granulites show tholeiitic affinity (Supplementary Figure S1a) representing continental tholeiitic basalt (Supplementary Figure S1b−c). The abundances of trace elements in Group-1 charnockites vary widely, e.g. Ni: 2.74−5.67 ppm, Co: 2.80−5.96 ppm, Cr: 11.30-35.59 ppm, V: 7.83−20.11 ppm, Sc: 6.21−8.53 ppm. With the exception of vanadium (17.85−22.19 ppm), trace element abundances in the Group-2 charnockites describe narrow ranges Ni: 3.38−3.65 ppm, Co: 4.18–6.54 ppm, Cr: 16.39−19.71 ppm, Sc: 6.21−8.53 ppm. By comparison, the Group-3 charnockites and granite gneisses have lower abundances of these elements (Ni: 1.31−1.73 ppm, Co: 1.86–2.22 ppm, Cr: 8.31−11.14 ppm, V: 6.34–7.62 ppm and Sc: 2.15– 4.51 ppm). Relative to the charnockites, the mafic granulites have high concentrations of transitional elements (Ni: 22.75−70.95 ppm, Co: 24.22−54.35 ppm, Cr: 57−195.37 ppm, V: 140.17−385.84 ppm and Sc: 23.28−53.06 ppm).

The Group-2, Group-3 charnockites and granite gneisses have low K/Rb ratios (average <200) relative to the Group-1 charnockites. The mean K/Rb ratio of 1108 in the Group-1 charnockites is higher than the average continental igneous rocks (Shaw 1968). The K/Rb ratios of mafic granulite show a wide range (506−1303) with an average value of 904 higher than the average value of crustal rocks. The primitive mantle-normalized (Sun and McDonough 1989) multi-element plots in spider diagram show prominent negative anomalies in Cs, Nb−Ta, Ce, Sr and Ti, and positive anomalies in Th, La, Pb, Nd, Sm and Gd (Figure 8a) in Group-1 charnockites. The Group-2 charnockites show similar (as in Group-1) trends in multi-element abundance diagram (Figure 8a), but exhibit enrichments in LILE and REE with considerable troughs between large ion lithophile (LILE) and high field strength (HFSE) elements (Figure 8a). However, Group-3 charnockites and granite gneisses display depletion in Cs, Ba, Nb-Ta, Sr, Zr-Hf, and Ti, and are enriched in Rb, Pb, Nd and Sm (Figure 8a). However, both the rocks follow similar trend for LILE and HFSE as in the Group-2 charnockites. This supports the view that Group-3 charnockites and granite gneisses belong to similar magmatic suite in comparison to the Group-1 and Group-2 charnockites (Figure 8a). In N-MORB normalized multi-element diagram (Sun and McDonough 1989), mafic granulites show enrichment in LILE and a prominent depletion of Nb, Sr, Zr and Ti, and positive anomalies of Pb, Nd, Sm and Y in (Figure 8b).

In chondrite-normalized (after Sun and McDonough 1989) abundance plots, the Group-1 charnockite samples show weak fractionation between the light rare earth elements (LREE) and the heavy rare earth elements (HREE), with slight depletion [$(La/Yb)_N$= 4.07−6.64] and higher fractionation between the LREEs [$(La/Sm)_N$= 2.52−4.57] as compared to the HREEs [$(Gd/Yb)_N$= 1.25−1.47] (Figure 8c). However, two samples (NGB-103 & NGBP-9B) display relatively higher REE fractionation [$(La/Yb)_N$= 13.09−34.18] showing HREE depletion [$(Gd/Yb)_N$= 2.09−5.42] (Figure 8c). Most of the samples show negative Eu anomaly [Eu/Eu*= 0.45−0.55] most likely suggesting fractionation by plagioclase in the source. On the other hand, one sample (NGBP-9B) displays positive Eu anomaly [Eu/Eu*= 1.88] with low ∑REE (125.8) suggesting plagioclase accumulation (Figure 8c) which relates to the formation of vein charnockites within mafic granulites (Figure 2c). The Group-2 charnockites exhibits high contents of LREE (La_N= 386−530 ppm) and HREE (Yb_N = 39−55 ppm) compared to the Group-1 charnockites. The LREE to HREE fractionation in the Group-2 charnockites exhibit weakly fractionated REE pattern [$(La/Yb)_N$= 7.01−11.27] with almost flat HREE pattern [$(Gd/Yb)_N$= 1.35−1.72] (Figure 8c; Table 3). The Group-2 charnockites show negative Eu-anomalies (0.35−0.46) (Figure 8c; Table 3) identical to those in Group-1 charnockites, except the sample showing positive Eu anomaly.

The Group-3 charnockites and granite gneisses exhibit moderately fractionated LREE pattern [$(La/Yb)_N$= 5.87−7.04; average 6.44] and relatively flatter HREE patterns [$(Gd/Yb)_N$ = 1.53−1.66; average 1.59) (Figure 8c). Further, prominent lower degree of negative Eu anomalies (Eu/Eu* = 0.28−0.34; average 0.32) are the characteristics of both the rocks (Table 3). The chondrite normalized (Sun and McDonough 1989) REE diagram of mafic granulites exhibit more or less flat REE pattern with moderate negative Eu-anomalies (0.78−0.88). The LREE fractionation [$(La/Sm)_N$= 1.44−1.67] and HREE fractionation [$(Gd/Yb)_N$ = 0.75−1.00) are nearly similar and less fractionated than those of charnockites (Figure 8d)

In FeO_t/MgO vs (Zr+Nb+Ce+Y) and Ce vs 10000*Ga/Al plots after Whalen et al. (1987), all varieties of charnockites (except a few samples) and granite gneiss plot in the field of A-type granitoids (Figure 9a,b). Further, Eby (1992) classified the A-type granitoids into two chemical divisions, namely A_1 and A_2 based on tectonic environments of magma derivation. On (Ce-Nb-Y) and (3*Ga-Nb-Y) plots (Eby, 1992), the charnockites and the granite gneisses plot in the field of A_2 type (Figure 9c, d) suggesting a post-collision continental tectonic setting or post-orogenic setting. All igneous charnockites (Group-2 and 3) and granite gneisses plot in the field of within-plate granite (Figure 9e; Pearce et al. 1984) as well as within the post-collisional granite field (Pearce 1996). The majority of Group-1 charnockites overlap with the field of post-collisional granites and volcanic arc granites or ocean ridge granites (Figure 9e). In the tectonic discrimination diagram of Shervais (1982), all mafic granulites correspond to continental flood basalt (Figure 9f).

Monazite Chemical Dating

In the present study, the samples (Tables 2 and 3) considered for P-T estimations and geochemical studies were devoid of monazite or contain extremely fine grained monazites (3−4 μm). Therefore, monazite chemical dating couldn't be performed in these samples. For that, petrographically constrained well-developed monazite (50−150μm) bearing samples from Group-1 charnockite (MAW-201 and MAW-108) and Group-2 charnockite (NGB-401) were selected for in-situ monazite dating after careful examination of scanning electron microscope BSE imaging and EDS analyses. Monazites in the selected samples (MAW-201, MAW-108 and NGB-401), collected from neighboring Nongstoin, are sub-idioblastic to xenoblastic in shape (Figure 10a-m).Fractured xenoblastic grains are also observed.

Monazites occur within orthopyroxene (Figure 10a), or share the boundaries with orthopyroxene (Figure 10b). Matrix monazites occur at the grain/phase boundaries of plagioclase, K-feldspar, quartz and biotite (Figure 10 c & l; d & k), and within plagioclase, K-feldspar and quartz (Figure 10f). Monazites in association with K-feldspar lamellae within antiperthite are rarely preserved in these samples (Figure 10c). Locally, monazites are in contact with ilmenite and magnetite (Figure 10e & g). The monazite compositions, the calculated spot ages and ±2σ errors are provided in the Supplementary table S2.

Most of the monazite grains display complex chemical zoning with irregular boundaries (Figure 10g-m). Only few monazite grains that occur within or at the contact with orthopyroxene do not exhibit any internal zoning. BSE and X-ray element images (Th, Y and U) of selected monazite grains illustrated (Figure 11a, b, d and e) that core portion of monazites have high ThO_2 content (10.97−16.93 wt%); the high-Th cores are mantled successively by zones of intermediate Th-content (ThO_2: 8.94–6.34 wt%) with irregular outlines, and low-Th domains (5.87–3.13 wt%) at the rims of the monazite grains. The Y_2O_3 contents in all monazites taken together and regardless of the associated minerals ranges between 1.09 and 3.79 wt%. The high-Th cores in most monazite grains have low-Y abundances, and are mantled by domains of increasing Y (Figure 11a–e). Grain 'c' in Figure 11 exhibit zone of high-Th (ThO_2: 8.70–8.87 wt.%) and U (UO_2: 0.16–0.18 wt.%) contents. The chemical heterogeneity in the monazites can be explained by solid solution along monazite-huttonite line in Th+U+Si vs P+Y+REE plot (Figure 12).

A total of 65 spot analyses were performed in monazites in the three samples; the analyses yielded apparent ages from 457 Ma to 566 Ma, with 2σ errors varying between from 17 Ma and 65 Ma. The statistically significant probable peak ages are calculated to be 501 ± 7 Ma (MSWD = 0.68; Figure 13a, b), 500 ± 6 Ma (MSWD = 0.95; Figure 13c, d) and 510 ± 8

Ma (MSWD = 0.71; Figure 13e, f) in MAW-201 (n = 24), NGB-401 (n = 27) and MAW-108 (n = 18), respectively.

Discussion

The low concentration of Ti and Y and high $[La/Yb]_N$ in the Group-1 charnockites suggest the likely retention of residual garnet, titanite and/or ilmenite in the source region. This is consistent with the HREE depletion trend shown by a number of charnockites samples (cf. Barker and Arth 1976; Sheraton and Black 1983). The element patterns suggest that the Group-1 charnockites formed by the partial melting of metabasic lower crustal rocks such as garnetiferous amphibolite. Also, the low abundances of LILE and the highly fractionated REE patterns in the Group-1 charnockites compared to the other two groups of charnockites suggest retention of garnet and/or hornblende as a residual phase in the source region (Drummond and Defant 1990; Martin et al. 2005). It is suggested that the protoliths for Group-1 charnockites formed by the partial melting of hydrated metamorphosed basaltic rocks (Rapp et al. 1991; Smithies et al. 2003; Martin et al. 2005). This inference is supported by the high Sr/Y and $[La/Yb]_N$ ratios in the Group-1 charnockites, where the involvement of partial melting of a hydrated metabasalt (low-K_2O) crust, with amphibole and/or garnet as a residual phases (Drummond and Defant 1990; Rapp et al. 1991; Martin et al. 2005). Moreover, these elevated ratios are the consequences of fractionation by plagioclase at source (Martin et al. 2005; Moyen 2009) which corroborates with the negative Sr-anomalies in multi-element plot (Figure 9a). This suggests that plagioclase was probably a residual phase during the generation of protolith by partial melting (Martin 1999). In addition, from the petrogenetic models of Patiño Douce (1999), it is possible to decipher that the origin of the protolith of Group-1 charnockites (tonalitic to granodioritic composition) related to partial melting of garnet amphibole bearing basaltic crust (Figure 9g–h).

The flat HREE patterns in the Group-2 charnockites [$(Gd/Yb)_N$ = 1.35−1.72] and the Group-3 charnockites [$(Gd/Yb)_N$ = 1.53−1.59], and the relatively high Y and Yb contents (Y: 70.59−110.55 ppm and Yb: 6.60–9.35 ppm in the Group-2 charnockites; Y: 102.28−134.70 ppm and 8.21−12.21 ppm in the Group-3 charnockites and granite gneisses) indicate that the rocks were derived from garnet-free protoliths.

The retention of plagioclase in the residual assemblage is characterized by marked negative Eu-anomalies (Kemp and Hawkesworth 2003; Martin and Moyen 2002) which also indicates melting under low aH_2O conditions (Tepper et al. 1993). As compared to the Group-1 charnockites, the high Rb/Sr and the Ba/Sr ratios noted in the Group-2, Group-3 charnockites and associated gneisses suggest a crustal source, particularly tonalite to granodiorite lithologies (Ravindra Kumar and Sreejith 2016). The crustal sources of the Group-2 and the Group-3 charnockites and the associated gneisses are favoured because the high-K, A-type nature of the granitoids precludes formation by partial melting of metabasic rocks (low-K_2O) (e.g. Roberts and Clemens 1993). This is also evident from the fact that these rocks are post-orogenic within plate granite as reflected from their plots in tectonic discrimination diagram (Figure 9e). Further, the presence of normative corundum and the peraluminous nature of the Group-3 charnockites indicate that Group-2 charnockites may have been chemically modified by contamination of crustal sources.

Similar to the charnockites, the mafic granulites show LILE enrichment with prominent positive anomalies in Pb and negative Sr anomalies. A prominent positive anomaly in Pb and negative Nb anomaly probably suggest a crustal influence. Flat chondrite normalized REE patterns with $\sum$REE =31−110 ppm, $(La/Lu)_N$ = 1.33−1.59 and Eu/Sm = 0.28−0.32 are features of a continental tholeiite (O'Nions and Clarke 1972; Alexander and

Gibson 1977; Frey et al. 1978). Unlike the charnockites, the mafic granulites do not show Nb–Ta troughs. Thus, the charnockite source rocks must have been enriched by LILE and REE and thus differ from these mafic granulites; alternately, hornblende fractionation might cause the observed Nb–Ta troughs in charnockites. Except the Nb depletion, the HFSE show a more or less flat pattern towards the right side of multi-element plots (Figure 8c). The low degree of negative Sr, Ti and Zr anomalies could be attributed to plagioclase, Ti-magnetite/ilmenite and zircon fractionation. The high values and wide variations of K/Rb ratios (506–1303) in mafic granulites are significantly higher than normal crustal value (~250) and can't be primary igneous feature. The mantle-derived mafic magmas at the time of upwelling can interact with the continental crust, but the negative Zr anomaly and the relatively low Hf concentration that are enriched in crustal material suggests no involvement of crustal contamination. In addition, the Cr (57–195.37 ppm) and Ni (22.75–70.95 ppm) concentrations in mafic granulites are very insignificant as compared to the primary mantle-derived magmas (Ni > 400–500 ppm, Cr > 1000 ppm) but limited analytical data precludes the production of primary magmas by either partial melting or/and fractional crystallization.

Summarizing, therefore, it appears that garnet and amphibole bearing mafic rocks were the protoliths for Group-1 charnockites. By contrast, the Group-2 and the Group-3 charnockites formed by intra-crustal melting of crustal sources involving removal of K-rich melt (granites). The inference is consistent with the findings of Kumar et al. (2017a) that several episodes of multiple melt production and granitoid emplacement characterized the SMGC. The mafic granulites resembling continental tholeiites experienced little or no crustal contamination.

Concluding Remarks

The results of mineral thermo-barometry and analyses of P-T pseudosection in the NCKFMASHTO system indicate that the chemically diverse charnockites formed by mid-crustal ultra-high temperature (>900 ºC) partial melting from different protoliths, including amphibolites. These high-T A_2-type charnockites are generated by partial melting of middle to lower crust in a post-collisional tectonic environment. The tightly constrained Cambrian-age (503 ± 4 Ma; MSWD=0.84) of emplacement of these charnockites attests to the prevalence of high temperature during the Pan-African orogenic crustal growth in the Shillong-Meghalaya Gneissic Complex. It is remarkable that the coeval nature of A-type Pan-African (~519–515 Ma) felsic-mafic magmatism in South Khasi Batholith (Kumar et al. 2017b) occurred to south of Sonapahar-Nongstoin domain. This felsic-mafic magmatism coincides well with chemically diverse charnockites during the period of post-collisional East Gondwana assembly- and growth-related accretion, after the cessation of amalgamation of fragmented components belonging to Rodinia supercontinents at approximately 550 Ma (e.g. Meert and VanDer Voo 1997). Further, it is likely to occur at a late stage tectonothermal events of the Pan-African-Brasiliano orogenic cycle, closely linked to the assembly of Gondwana supercontinents. Conversely, it has been argued by Khonglah et al. (2022) that the tectonic settings during Pan-African orogeny is a continental arc margin which may cause crustal thickening and subsequent thinning due to terrain exhumation probably followed by lower crust and upper lithospheric mantle upwelling that was accompanying the closing of the Shillong Group basin. Evidences for upwelling are indicated by intrusion of the Khasi meta-mafic rocks (erstwhile Khasi Greenstone), norite, noritic gabbros, monzogabbros, monzodiorites, diorite and lamprophyric rocks (Ray et al. 2013; Hazra et al. 2015; Khonglah et al. 2022). The association of norite, noritic gabbros, monzogabbros, monzodiorites and diorite with both metamorphic and magmatic charnockites, suggest that they are the bearers of CO_2 laden fluids that promoted charnockitisation along major deep seated lineaments, joints and shear zones through degassing processes in Central SMGC (Khonglah et al. 2018; 2022). The charnockitisation event was successively followed by large scale porphyritic granitoids in the South Khasi Batholith, Kyllang and Mawdoh Plutons between 430 Ma and 530 Ma (Kumar et al. 2017b) These granitoid magmas were generated by late stage decompression melting at mature continental arc margin (Winter 2014). But the collision zone responsible for this active continental margin is not known. Even this tectonic setting of active continental margin has also been supported by the charnockite magmatism related crustal growth of the Indian subcontinent particularly Southern Granulite Terrain and Eastern Ghats Belt (Rajesh 2012). But the geochemical characteristics of studied Pan-African charnockites from SMGC record a post-collisional tectonic environment. This is consistent with the finding in the Prydz Bay suture which is deemed to be an ultra-high temperature Pan-African accretion zone (Boger et al. 2001; Mikhalsky et al. 2001; Kelsey et al. 2008).

The Prydz Bay is characterized by predominantly high grade metamorphic rocks and abundant charnockites and granites (Liu et al. 2009). Charnockites in the East Antarctica were suggested to have emplaced in two different geological periods (~1.1–0.95Ga and ~ 0.6–0.5Ga), and show distinct compositional and mineralogical variation which may, to some extent, correspond to different tectonic settings (Mikhalsky et al. 2006). Published U-Pb (zircon) concordant dates (with $< 2\%$ discordance; Figure 14a) and monazite chemical dating (with 2σ errors less than 10%; Figure 14b) from the basement gneisses and intrusive granites of SMGC display the dominant tectonothermal events experienced by the SMGC. In contrast, Borah et al. (2019) mentioned that the late Cambrian event representing ubiquitous Pan-African granulite facies tectonothermal event has highly affected the central and eastern portions of the SMGC which may obliterate the earlier events preserved in the monazites.

Further, the occurrence of both metamorphic and magmatic varieties of charnockites in SMGC raises concern on the single monazite age (~500 Ma) in the charnockites. Therefore, monazite U-Th-Pb_{total} ages cannot be explicitly used to infer single stage charnockitization (~500 Ma) in the SMGC, and such consideration may obscure significant petrogenetic information of the charnockites and tectonic framework of their formation.

Acknowledgments

This work is partially funded by University Grant Commission; Govt. of India sponsored Major Research Project MRP-MAJOR-GEOL-2013-36821 granted to ACM. The authors thank Prof. Biswajit Mishra for facilitating EPMA analyses in the DST-IIT National EPMA facility, IIT Kharagpur. The authors acknowledge the Director, CSIR-NGRI for providing the facility to carry out the major oxide whole rock analyses. All the authors thank Dr. Dewashish Upadhyay for facilitating trace element analyses at the Diamond Jubilee Radiogenic Isotope Facility, IIT Kharagpur. The Department of Geological Sciences, Gauhati University is acknowledged for the optical photomicrographs obtained through DST-FIST funding (SR/FST/ESI-152/2016) microscope-imaging facility.

Declarations

Ethical Approval

This declaration is not applicable.

Competing interests

The authors declare that there are no competing financial interests to disclose that are directly or indirectly related to the work reported in this paper.

Authors' Contributions

PB, ACM and A. Bhattacharya formulated the study. PB, ACM, BB and MAK carried out field work and rock sampling during the course of work. All authors carried out the petrographic studies in the laboratory. PB, ACM and BB conducted the processes during the analysis of EPMA data and in whole rock chemical analysis. All authors involved in plotting the analyzed data and prepared all the figures. PB, ACM, BB, MAK and A. Bhattacharya have equal contribution in interpreting data and writing the manuscript. All authors reviewed the manuscript and PB compiled the final manuscript.

Funding

University Grant Commission, Government of India sponsored Major Research Project bearing no. MRP-MAJOR-GEOL-2013-36821 granted to ACM.

Availability of data and materials

Supplementary information is attached as a separate DOCX file. Also, supplementary data and figure to this article are attached as separate tables in the XLSX format and as Bitmap file, respectively.

References cited

Alexander PO, Gibson IL (1977) Rare earth abundances in Deccan Trap basalts. Lithos 10:43−147

Anderson JL, Smith DR (1995) The effects of temperature and f_{O2} on the Al-in-hornblende barometer. Am Mineral 80(5-6):549−559

Barker F, Arth JG (1976) Generation of trondhjemitic–tonalitic liquids and Achaean bimodal trondhjemites-basalt suites. Geology 4:596–600

Bidyananda M, Deomurari MP (2007). Geochronological constraints on the evolution of Meghalaya massif, northeastern India: An ion microprobe study. Current Sci 93(11):1620−1623

Blundy JD, Holland TJ(1990) Calcic amphibole equilibria and a new amphibole-plagioclase geothermometer. Contrib Mineral Petrol 104(2):208−224

Boger SD, Wilson CJL, Fanning CM (2001) Early Paleozoic tectonism within the East Antarctic craton: The final suture between east and west Gondwana?. Geology 29(5):463−466

Borah P, Hazarika P, Mazumdar AC, Rabha M (2019) Monazite and xenotime U–Th–Pb_{total} ages from basement rocks of the (central) Shillong–Meghalaya Gneissic Complex, Northeast India. J Earth Syst Sci 128(3):1−20

Chatterjee N (2017) Constraints from monazite and xenotime growth modelling in the Mn CKFMASH-PYC e system on the P–T path of a metapelite from Shillong-Meghalaya Plateau: implications for the Indian shield assembly. J Metamorph Geol 35(4):393–412

Chatterjee N, Bhattacharya A, Duarah BP, Mazumdar AC (2011) Late Cambrian reworking of Paleo-Mesoproterozoic granulites in Shillong-Meghalaya gneissic complex (Northeast India): evidence from PT pseudosection analysis and monazite chronology and implications for East Gondwana assembly. J Geol 119(3):311−330

Chatterjee N, Mazumdar AC, Bhattacharya A, Saikia, RR (2007). Mesoproterozoic granulites of the Shillong–Meghalaya Plateau: evidence of westward continuation of the Prydz Bay Pan-African suture into Northeastern India. Precambrian Res 152(1-2):1−26

Choudhary AK, Harris NBW, Van Calsteren P, Hawkesworth CJ (1992) Pan-African charnockite formation in Kerala, south India. Geol Mag 129(3):257−264

Connolly JA (2005) Computation of phase equilibria by linear programming: a tool for geodynamic modeling and its application to subduction zone decarbonation. Earth Planet Sci Lett 236(1-2):524−541

Crawford AR (1974) Indo-Antarctica, Gondwana Land and pattern of the distortion of a granulite belt. Tectonophysics 22:141–157

Desikachar SV (1974) A review of the tectonic and geological history of eastern India in terms of plate tectonic theory. J Geol Soc India 15:137–149

Diener JFA, Powell R, White R W, Holland TJB (2007) A new thermodynamic model for clino-and orthoamphiboles in the system Na_2O–CaO–FeO–MgO–Al_2O3–SiO_2–H_2O–O. J Metamorph Geol 25(6):631−656

Doley D, Bhagabaty B, Sarma G, Singh AK, Zou X (2022) Geochemistry of Late Palaeoproterozoic (1.69 Ga) A-type Mayong granitoids in Shillong Plateau, north-east

India: Implication for anorogenic magmatism during Columbia Supercontinent cycle. Geol J 57(2):662−680

Drummond MS, Defant MJ (1990) A model for trondhjemite-tonalite-dacite genesis and crustal growth via slab melting: Archean to modern comparisons. J Geophys Res Solid Earth 95(B13): 21503−21521

Dwivedi SB, Theunuo K, Kumar RR (2020) Characterization and metamorphic evolution of Mesoproterozoic granulites from Sonapahar (Meghalaya), NE India, using EPMA monazite dating. Geol Mag 157(9):1409−1427

Eby GN (1992) Chemical subdivision of the A-type granitoids: petrogenetic and tectonic implications. Geology 20:641−644

Evans P (1964) The tectonic framework of Assam. J Geol Soc India 5:80–96

Frey FA, Green DH, Roy SD (1978) Integrated models of basalt petrogenesis: a study of quartz tholeiites to olivine melilitites from south eastern Australia utilizing geochemical and experimental petrological data. J Petrol 19(3):463−513

Frost BR, Frost CD (2008) On charnockites. Gondwana Res 13:30–44

Frost BR, Barnes CG, Collins WJ, Arculus RJ, Ellis DJ, Frost CD (2001) A geochemical classification for granitic rocks. J Petrol 42(11):2033−2048

Fuhrman ML, Lindsley DH (1988) Ternary-feldspar modeling and thermometry. Am Mineral 73:201−215

Gogoi K (1963) The geology of parts of the Khasi Hills along the southwestern and southeastern extension of the Sonapahar and structure of the main Sonapahar belt, Assam. Unpublished report of Geol Surv Intl Prog

Gogoi K (1975) The geology of the Precambrian rocks in northwest part of the Khasi and Jaintia Hills, Meghalaya. Miscellaneous Publications of the Geological Survey of India 23:37–48

Green E, Holland T, Powell R (2007) An order-disorder model for omphacitic pyroxenes in the system jadeite-diopside-hedenbergite-acmite, with applications to eclogitic rocks. Am Mineral 92(7):1181−1189

Hammarstrom JM, Zen EA (1986) Aluminum in hornblende: an empirical igneous geobarometer. Am Mineral 71(11-12):1297−1313

Hazra S, Ray J, Manikyamba C, Saha A, Sawant SS (2015) Geochemistry of PGE in mafic rocks of east Khasi Hills, Shillong plateau, NE India. J Earth Syst Sci 124(2):459–475

Henry DJ, Guidotti CV, Thomson JA (2005). The Ti-saturation surface for low-to-medium pressure metapelitic biotites: Implications for geothermometry and Ti-substitution mechanisms. Am Mineral 90(2-3):316−328

Holland TJB, Powell R (2011) An improved and extended internally consistent thermodynamic dataset for phases of petrological interest, involving a new equation of state for solids. J Metamorph Geol 29(3):333−383

Hollister LS, Grissom GC, Peters EK, Stowell HH, Sisson VB (1987) Confirmation of the empirical correlation of Al in hornblende with pressure of solidification of calc-alkaline plutons. Am Mineral 72(3-4):231−239

Kelsey DE, Wade BP, Collins AS, Hand M, Sealing CR, Netting A (2008) Discovery of a Neoproterozoic basin in the Prydz belt in East Antarctica and its implications for Gondwana assembly and ultrahigh temperature metamorphism. Precambrian Res 161(3-4):355−388

Kemp AIS, Hawkesworth CJ (2003) Granitic perspectives on the generation and secular evolution of the continental crust. In: Rudnick RL (Ed.) The Crust. Treatise on Geochemistry, Elsevier–Pergamon, Oxford, 3, pp 349–410

Khonglah MA, Khan MA, Karim MA, Kumar A, Choudhury J (2008) Geology and structure of the areas in and around Shillong, Meghalaya, north East India, revisited, proceedings of the National Seminar on Geology & Energy Resources of NE India: Progress & Perspectives Nagaland University Research Journal Special Publication (pp. 115−139)

Khonglah MA, Kumar AA, Haokip L, Sougrakpam S, Imchen I (2022) Geochemistry of meta-mafic and meta-tonalite-trondhjemite intrusives from Jaintia and Karbi Anglong hills of Shillong Plateau, North East India: Implications on the evolution of the Proterozoic Shillong Basin. Geol J 57(12):5097−5126

Khonglah MA, Mohapatra SR, Imtikumzuk (2010) Final Report on Specialized Thematic Mapping of Gabbroic Anorthosite and the associated Porphyritic Granite around Nongkasen-Nongstoin and Myriaw-Synnia area along with parentage studies of Gabbroic Anorthosite rock, West Khasi Hills, Meghalaya, GSI, Unpublished Report F.S. 2007-09

Khonglah MA, Theunuo K, Mukherjee P, Gupta S, Tripathy SK, Sougrakpam S (2018) Study on fluid-controlled charnockitization of granite-gneiss in parts of west Khasi Hills district, Meghalaya. GSI, NER, e-news. Vol. 28(i)

Kilpatrick JA, Ellis DJ (1992) C-type magmas: igneous charnockites and their extrusive equivalents. Earth Environ Sci Trans R Soc Edinb 83(1-2):155–164

Kretz R (1983) Symbols for rock-forming minerals. Am Mineral 68(1-2):277−279

Kumar S, Pieru T, Rino V, Hayasaka Y (2017b) Geochemistry and U–Pb SHRIMP zircon geochronology of microgranular enclaves and host granitoids from the South Khasi Hills of the Meghalaya Plateau, NE India: evidence of synchronous mafic–felsic magma mixing–fractionation and diffusion in a post-collision tectonic environment during the Pan-African orogenic cycle. Geol Soc Lond Spec Publ 457(1):253−289

Kumar S, Rino V, Hayasaka Y, Kimura K, Raju S, Terada K, Pathak M (2017a) Contribution of Columbia and Gondwana Supercontinent assembly-and growth-related magmatism in the evolution of the Meghalaya Plateau and the Mikir Hills, Northeast India: Constraints from U-Pb SHRIMP zircon geochronology and geochemistry. Lithos 277:356–375

Lal RK, Ackermand D, Seifert F, Haldar SK (1978) Chemographic relationships in sapphirine-bearing rocks from Sonapahar, Assam, India. Contrib Mineral Petrol 67(2):169−187

Liu X, Zhao Y, Song B, Liu J, Cui J (2009) SHRIMP U–Pb zircon geochronology of high-grade rocks and charnockites from the eastern Amery Ice Shelf and southwestern Prydz Bay, East Antarctica: constraints on Late Mesoproterozoic to Cambrian tectonothermal events related to supercontinent assembly. Gondwana Res 16(2):342−361

Ludwig KR (2012) Isoplot 4.15: A Geochronological Toolkit for Microsoft Excel. Berkeley, California: Berkeley Chronological Center, Special Publication 5 pp

Majumdar D, Dutta P (2016) Geodynamic evolution of a Pan-African granitoid of extended Dizo valley in Karbi Hills, NE India: Evidence from geochemistry and isotope geology. J Asian Earth Sci 117:256–268

Martin H (1999) Adakitic magmas: modern analogues of Archaean granitoids. Lithos 46(3):411−429

Martin H, Moyen JF (2002) Secular changes in tonalite-trondhjemite-granodiorite composition as markers of the progressive cooling of Earth. Geology 30(4):319−322

Martin H, Smithies RH, Rapp R, Moyen JF, Champion D (2005) An overview of adakite, tonalite–trondhjemite–granodiorite (TTG), and sanukitoid: relationships and some implications for crustal evolution. Lithos 79(1-2):1−24

Mazumdar SK (1976) A summary of the Precambrian Geology of Khasi Hills, Meghalaya. Geol Surv India Misc Publ 23:311–334

Meert JG, VanDer Voo R (1997) The assembly of Gondwana 800–550 Ma. J Geodyn 23:223–235

Mikhalsky EV, Sheraton JW, Beliatsky BV (2001) Preliminary U-Pb dating of Grove Mountains rocks; implications for the Proterozoic to Early Palaeozoic tectonic evolution of the Lambert Glacier-Prydz Bay area (East Antarctica). Terra Antartica 8(1):3−10

Mikhalsky EV, Sheraton JW, Hahne K (2006) Charnockite composition in relation to the tectonic evolution of East Antarctica. Gondwana Res 9(4):379−397

Miller JS, Santosh M, Pressley RA, Clements AS, Rogers JJW (1996) A Pan-African thermal event in southern India. J Southeast Asian Earth Sci 14(3-4):127−136

Moyen JF (2009) High Sr/Y and La/Yb ratios: the meaning of the "adakitic signature". Lithos 112(3-4):556−574

Mueller RF, Saxena SK (1977) Chemical Petrology: with applications to the Terrestrial Planets and Meteorites. Springer-Verlag New York, 394 pp

Nandy DR (2001) Geodynamics of northeastern India and the adjoining region. ACB Publications, Kolkata, India, 209 pp

Nedelec A, Ralison B, Bouchez JL, Gregoire V (2000) Structure and metamorphism of the granitic basement around Antananarivo' A key to the Pan-African history central Madagascar and its Gondwana connections. Tectonics 19:997−1020

Newton RC (1992) Charnokitic alteration: evidence for CO_2 infiltration in granulite facies metamorphism. J Metamorph Geol 10:383–400

O'nions RK, Clarke DB (1972) Comparative trace element geochemistry of Tertiary basalts from Baffin Bay. Earth Planet Sci Lett 15(4):436−446

Pascoe EH (1950) A manual of the geology of India and Burma. Geological Survey of India (Third Edition reprinted in 1973) Vol I, pp 239–244

Patiño Douce AE (1999) What do experiments tell us about the relative contributions of crust and mantle to the origin of granitic magmas? In: Castro A, Fernandez C, Vigneressese JL (Eds.) Understanding Granites: Integrating New and Classical Techniques. Geol Soc Lond Spec Publ 168:55–75

Pearce JA (1996) Sources and settings of granitic rocks. Episodes 19(4):120–125

Pearce JA, Harris NB, Tindle AG (1984) Trace element discrimination diagrams for the tectonic interpretation of granitic rocks. J Petrol 25(4):956-983

Pichamuthu CS (1960) Charnockite in the making. Nature 188:135–136

Praharaj P, Rekha S, Bhattacharya A (2021) Structure and chronology across the Achankovil terrain boundary shear zone system (South India), and its Madagascar connection in the Gondwanaland. Int J Earth Sci 110:1545–1573

Rajesh HM (2012) A geochemical perspective on charnockite magmatism in Peninsular India. Geosci Front 3(6):773-788

Rajesh HM, Santosh M (2012) Charnockites and charnockites. Geosci Front 3(6):737–744

Rapp RP, Watson EB, Miller CF (1991) Partial melting of amphibolite/eclogite and the origin of Archean trondhjemites and tonalites. Precambrian Res 51(1-4):1–25

Ravindra Kumar GR, Sreejith C (2016) Petrology and geochemistry of charnockites (felsic ortho-granulites) from the Kerala Khondalite Belt, Southern India: Evidence for intra-crustal melting, magmatic differentiation and episodic crustal growth. Lithos 262:334–354

Ray J, Saha A, Koeberl C, Martin T, Ganguly S, Hazra S (2013) Geochemistry and petrogenesis of Proterozoic mafic rocks from east Khasi Hills, Shillong plateau, Northeastern India. Precambrian Res 230:119–137

Rickwood PC (1989) Boundary lines within petrologic diagrams which use oxides of major and minor elements. Lithos 22(4):247–263

Roberts MP, Clemens J D (1993) Origin of high-potassium, calc-alkaline, I-type granitoids. Geology 21(9):825–828

Sadiq M, Umrao RK, Sharma BB, Chakraborti S, Bhattacharyya S, Kundu A (2018) Mineralogy, geochemistry and geochronology of mafic magmatic enclaves and their significance in evolution of Nongpoh granitoids, Meghalaya, NE India. Geol Soc Lond Spec Publ 463(1):171–198

Santosh M, Omori S (2008) CO2 flushing: a plate tectonic perspective. Gondwana Res 13:86–102

Schmidt MW (1992) Amphibole composition in tonalite as a function of pressure: an experimental calibration of the Al-in-hornblende barometer. Contrib Mineral Petrol 110(2-3):304–310

Sen SK, Ray S (1971a) Hornblende-pyroxene granulites versus pyroxene granulites: a study from the type charnockite area. Neues Jahrb Mineral Abh 115:291–314

Sen SK, Ray S (1971b) Breakdown reactions for natural hornblendes in granulite facies. Neues Jahrb Mineral Abhandl 115:301–319

Shand SJ (1943) The Eruptive Rocks, 2nd edn, John Wiley and Sons, New York, 444 pp

Shaw DM (1968) Radioactive elements in the Canadian Precambrian shield and the interior of the earth. In Origin and Distribution of the Elements, Pergamon, pp 855–870

Sheraton JW, Black LP (1983) Geochemistry of Precambrian gneisses: relevance for the evolution of the East Antarctic Shield. Lithos 16(4):273–296

Shervais JW (1982) Ti-V plots and the petrogenesis of modern and ophiolitic lavas. Earth Planet Sci Lett 59(1):101–118

Smithies RH, Champion DC, Cassidy KF (2003) Formation of Earth's early Archaean continental crust. Precambrian Res 127(1-3):89–101

Streckeisen A (1974) Classification and nomenclature of plutonic rocks recommendations of the IUGS subcommission on the systematics of igneous rocks. Geologische Rundschau 63(2):773−786

Stüwe K, Braun HM, Peer H(1989) Geology and structure of the Larsemann Hills area, Prydz Bay, East Antarctica. Aust J Earth Sci 36:219−241

Sun SS, McDonough WF (1989) Chemical and isotopic systematics of oceanic basalts: implications for mantle composition and processes. In: Saunders A D, Norry MJ (Eds.) Magmatism in the Ocean Basins. Geol Soc Lond Spec Publ 42:313–345

Taylor SR, McLennan SM (1985) The continental crust: its composition and evolution. Blackwell Scientific Publications, Oxford, 312 pp

Tepper JH, Nelson BK, Bergantz GW, Irving AJ (1993) Petrology of the Chilliwack batholith, North Cascades, Washington: generation of calc-alkaline granitoids by melting of mafic lower crust with variable water fugacity. Contrib Mineral Petrol 113(3):333−351

Tingey R J (1981) Geological investigations in Antarctica 1968–1969: The Prydz Bay-Amery Ice Shelf-Prince Charles Mountains area. Bureau of Mineral Resources, Geology and Geophysics, 144 pp

Touret JL, Huizenga JM (2012) Charnockite microstructures: from magmatic to metamorphic. Geosci Front 3(6):745−753

Tubosun IA, Lancelot JR, Rahaman MA, Ocan O (1984) U-Pb Pan-African ages of two charnockite-granite associations from southwestern Nigeria. Contrib Mineral Petrol 88:188−195

Wells PR (1977) Pyroxene thermometry in simple and complex systems. Contrib Mineral Petrol 62(2):129−139

Whalen JB, Currie KL, Chappell BW (1987) A-type granites: geochemical characteristics, discrimination and petrogenesis. Contrib Mineral Petrol 95:407−419

White RW, Powell R, Clarke GL (2002) The interpretation of reaction textures in Fe-rich metapelitic granulites of the Musgrave Block, central Australia: constraints from mineral equilibria calculations in the system K_2O–FeO–MgO–Al_2O_3–SiO_2–H_2O–TiO_2–Fe_2O_3. J Metamorph Geol 20(1):41−55

White RW, Powell R, Holland TJB, Johnson TE, Green ECR (2014) New mineral activity–composition relations for thermodynamic calculations in metapelitic systems. J Metamorph Geol 32(3) 261−286

Winter JD (2014) An introduction to igneous and metamorphic petrology (2nd ed.). Pearson Education Ltd

Wood BJ, Banno S (1973) Garnet-orthopyroxene and orthopyroxene-clinopyroxene relationships in simple and complex systems. Contrib Mineral Petrol 42(2):109−124

Wu CM, Pan Y, Wang K (1999) Refinement of the biotite-orthopyoxene geothermometer with applications. Acta Petrol Sin 15(3):463-468 (in Chinese with English abstract)

Yin A, Dubey CS, Webb AAG, Kelty TK, Grove M, Gehrels GE, Burgess WP (2010) Geologic correlation of the Himalayan orogen and Indian craton: Part 1. Structural geology, U-Pb zircon geochronology, and tectonic evolution of the Shillong Plateau and its neighboring regions in NE India. GSA Bulletin 122(3-4):336−359

Figures:

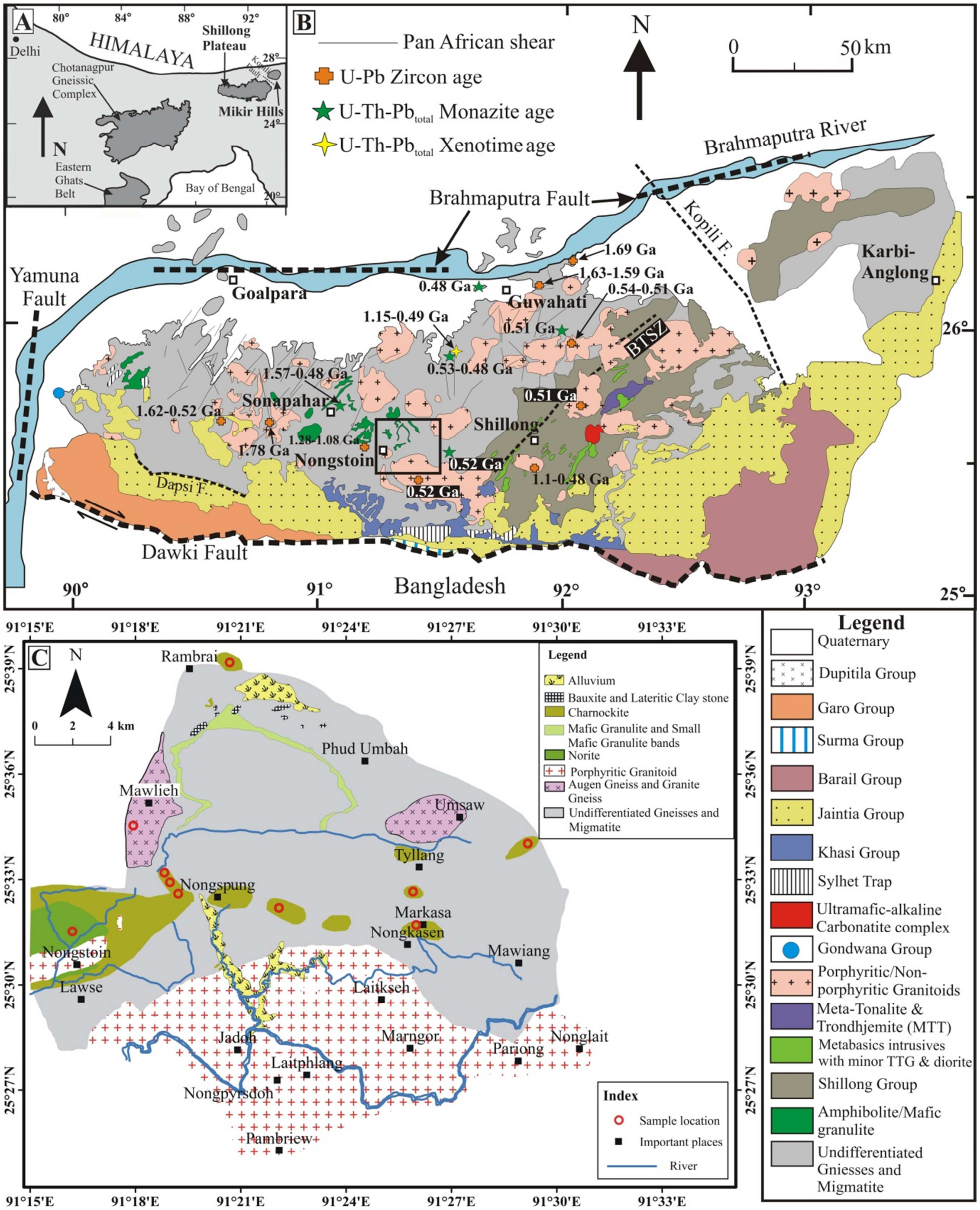

Fig. 1 *A, B*, Simplified regional geological map of the Shillong-Meghalaya Gneissic Complex (SMGC) modified after Khonglah et al. (2022) and reference therein. The numbers keyed to

the figure correspond to the U-Pb (zircon) concordant dates having < 2% discordance (Bidyananda and Deomurari 2007; Doley et al. 2022; Kumar et al. 2017a; 2017b; Yin et al. 2010), and monazite and xenotime chemical dates with 2σ errors less than 10% (Borah et al. 2019; Chatterjee et al. 2007; 2011; Dwivedi et al. 2020; Yin et al. 2010) (abbreviation *BTSZ* in figure B stands for Barapani-Tyrsad Shear Zone); *C*, Geological map along Nongstoin-Markasa-Rambrai road section modified after Khonglah et al. (2010), showing the disposition of the lithounits exposed in the study area. The location of map C is shown in B.

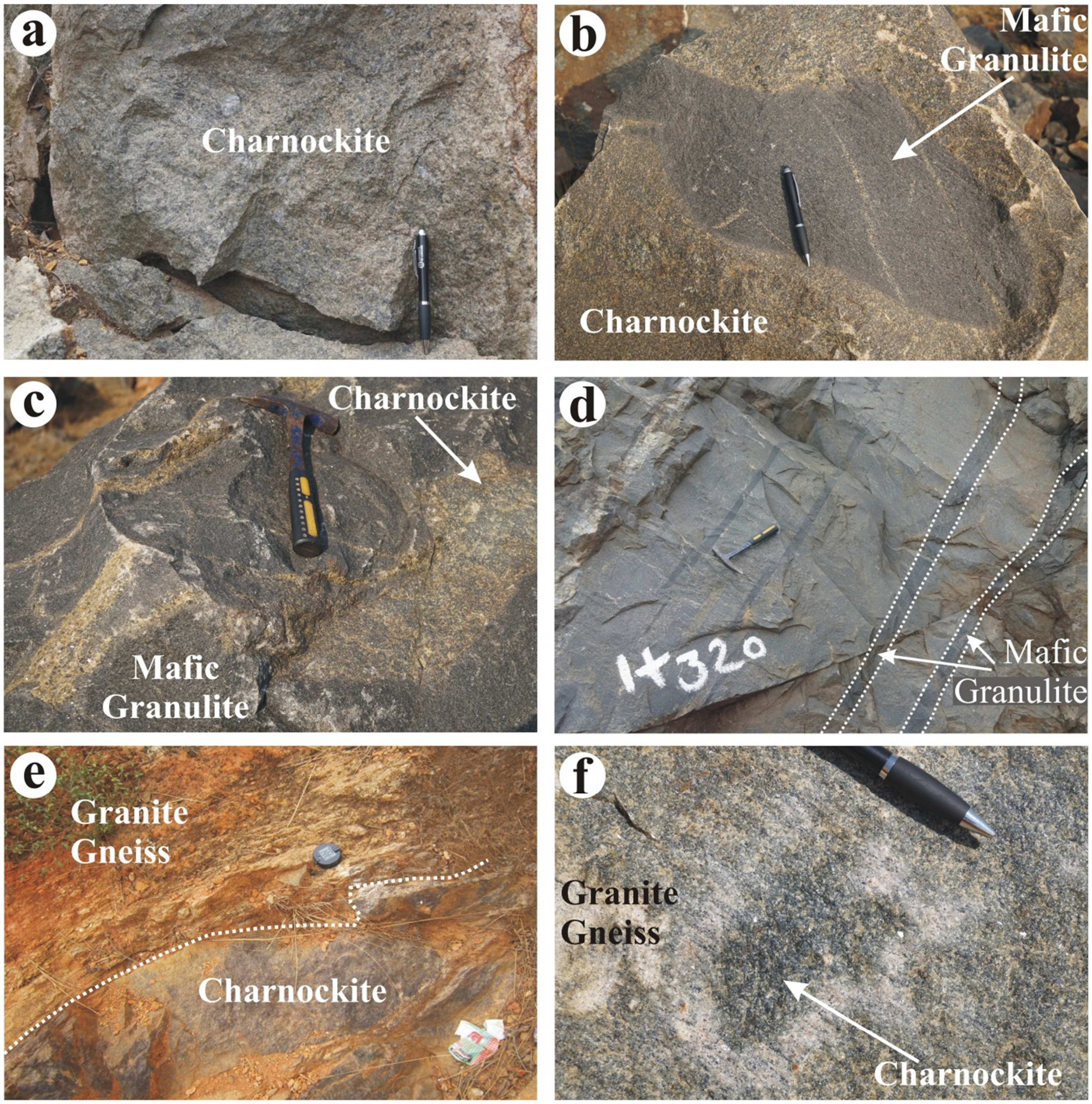

Fig. 2 Field photographs showing plan view section from Markasa-Nongstoin-Rambrai area: *a*, Coarse-grained massive charnockites; *b*, Irregular enclave of mafic granulite within charnockites; *c*, Apophyses of charnockites within mafic granulite; *d*, Bands of mafic granulites within charnockites; *e*, Charnockites associated with granite gneiss. Note the sharp contact between the two rocks; *f*, Irregular patchy charnockites within granite gneiss. Note the diffuse margin between the two rocks is continuous across the shared foliation.

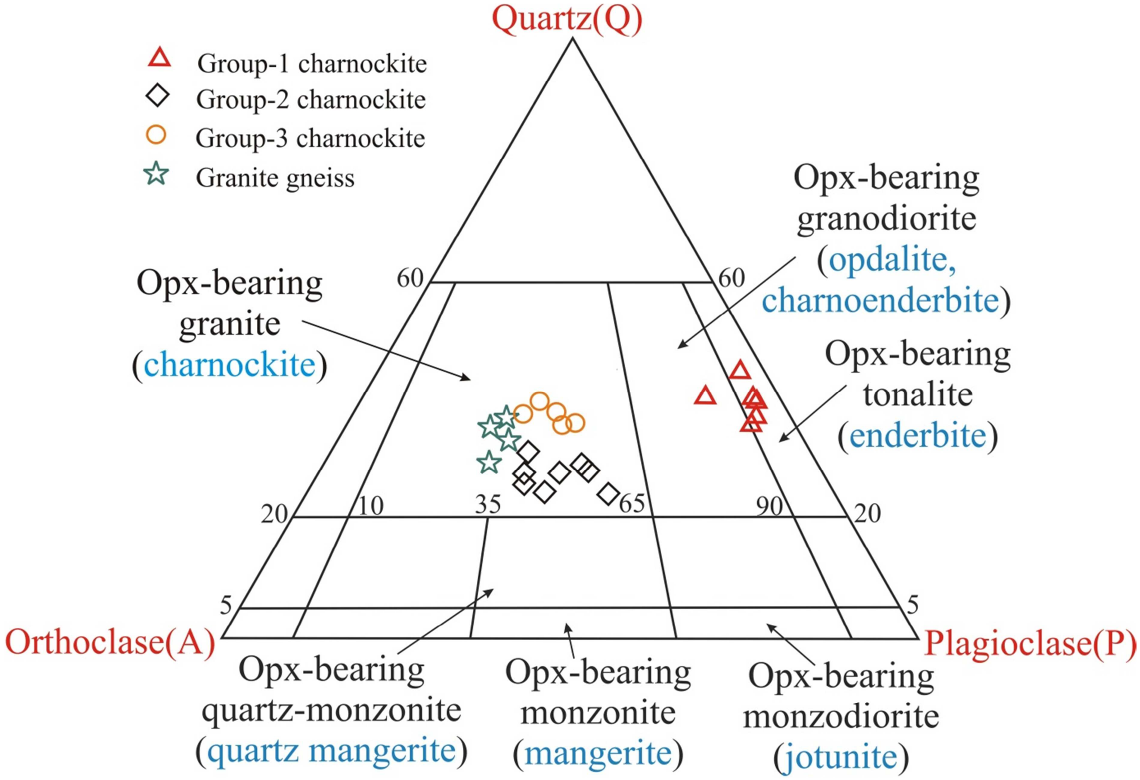

Fig. 3 Quartz-Alkali-feldspar-Plagioclase (QAP) diagram showing the modal proportions of the different varieties of charnockites and granite gneisses

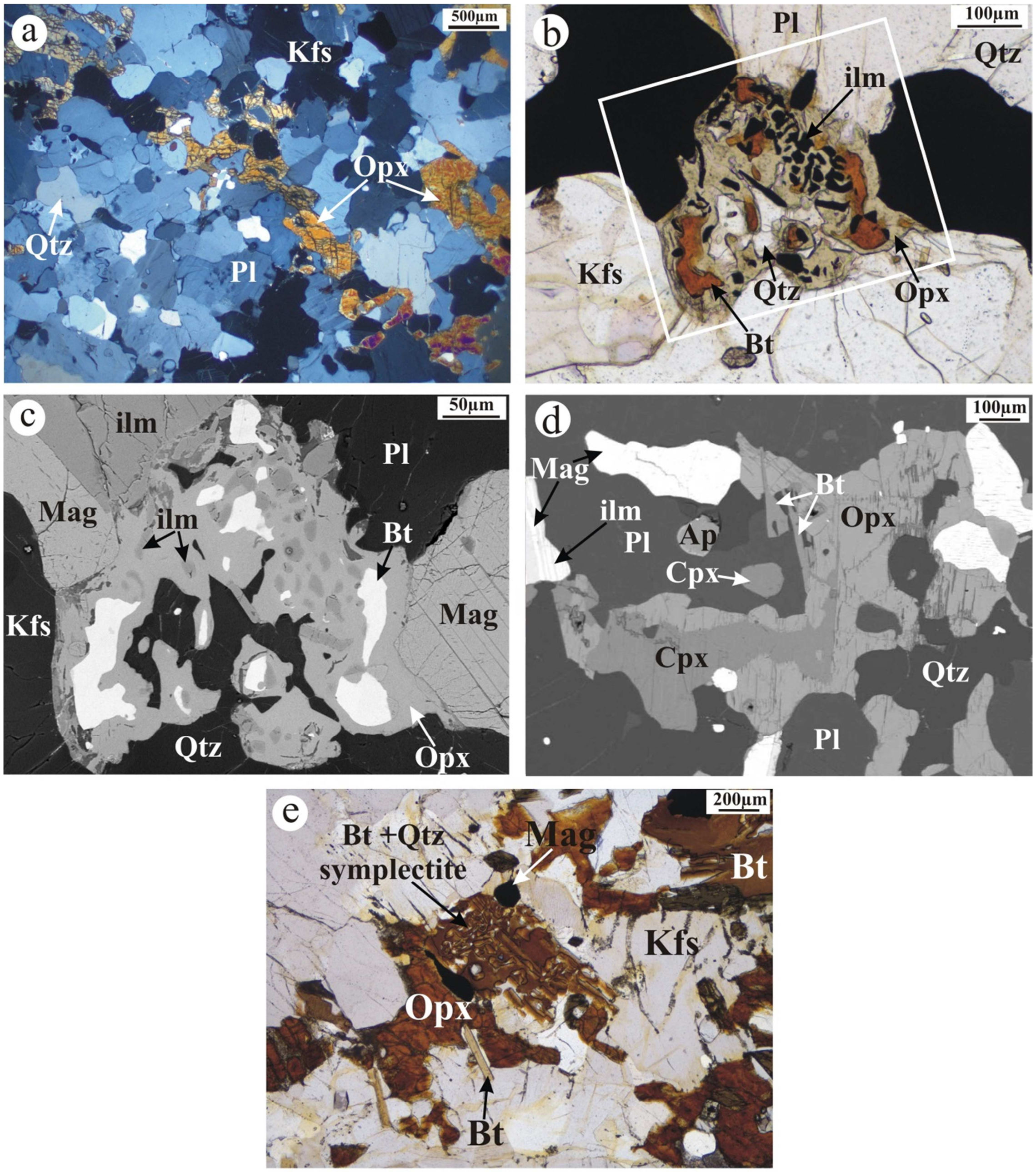

Fig. 4 Textures in charnockites: *a*, Crossed-polars image of linear aggregates of xenomorphic orthopyroxene grains defining the gneissic foliation in charnockite. Dynamic recrystallization manifested by polygonisation among quartz and feldspar grains overprints the foliation; *b* & *c*, Microphotograph and back-scattered electron (BSE) images of rare inclusions of biotite, ilmenite and quartz within orthopyroxene, respectively. Note that the box in figure b indicates the area of figure c; *d*, BSE image of boundary relationships among clinopyroxene,

orthopyroxene, plagioclase, quartz in metamorphic charnockite; *e*, Crossed-polars image of Group-1 metamorphic charnockites exhibiting biotite-quartz symplectite at orthopyroxene and K-feldspar boundary (mineral abbreviations after Kretz 1983).

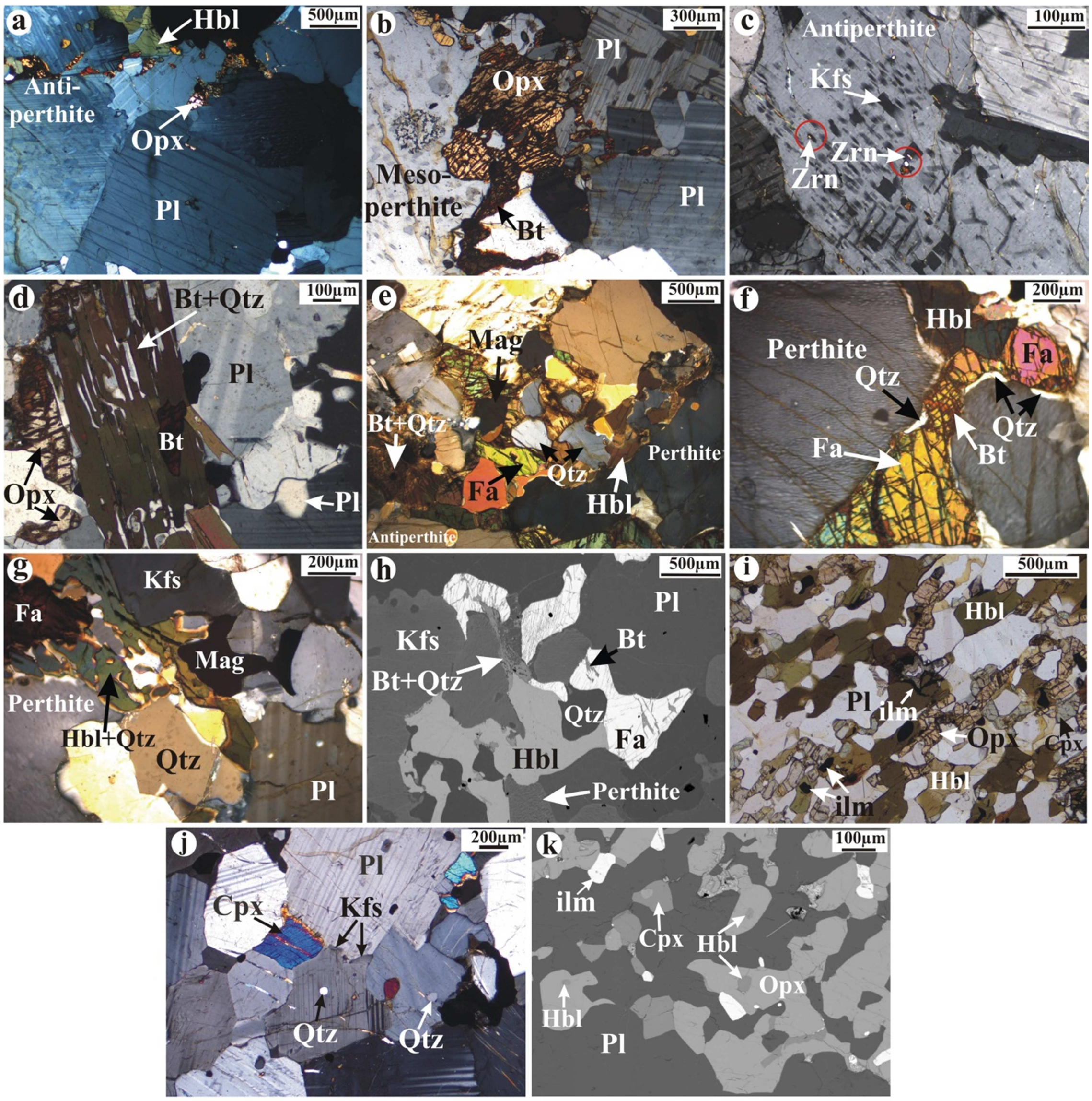

Fig. 5 Cross-polars images of textural relations in charnockites and mafic granulites: *a*, Euhedral to subhedral plagioclase, associated with anhedral grains of pyroxene and hornblende along the plagioclase grain boundaries; *b*, Intergrowth of pyroxene and

plagioclase; *c*, Tiny crystal of zircon (honey brown) hosted in antiperthite patch within plagioclase; *d*, Biotite + quartz symplectite at orthopyroxene margin, in the absence of K-feldspar; *e*, Fayalitic olivine and quartz intergrowth in Group-3 charnockite; *f*, Local presence of melt along the grain boundaries of fayalite presently represent as thin quartz veins; Photomicrograph 'g' and BSE image 'h' showing intergrowth of hornblende + quartz and biotite + quartz separating fayalite from plagioclase and K-feldspar, respectively. Photomicrographs and BSE image (i–k) showing textural settings of minerals in mafic granulites, *i*, concentration of ilmenite along margin/fracture/cleavage of hornblende; *j*, granoblastic polygonal texture in pyroxene granulites. Note: discrete grains of K-feldspar along plagioclase margin; *k*, BSE image displaying rare inclusions of hornblende and quartz (syn-S_1, M_1) within orthopyroxene (post-S_1, pre-S_2, M_2) in pyroxene granulite**.**

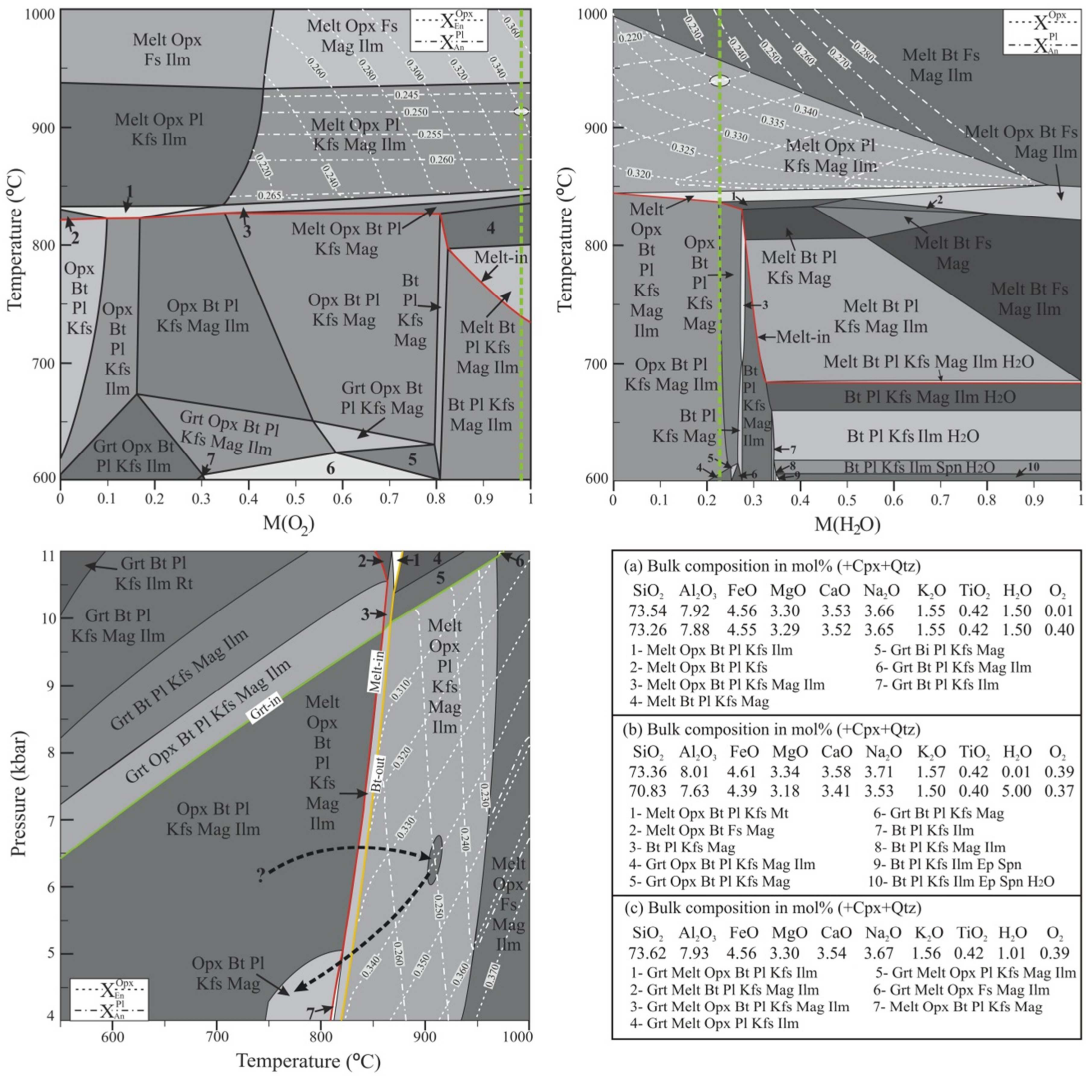

Fig. 6 NCKFMASHTO pseudosections for the metamorphic variety (Group-1) charnockite sample NGB-304: *a*, T-M(O_2) diagram and *b*, T-M(H_2O) diagram computed at 7 kbar; *c*, P-T pseudosection calculated at the adjusted H_2O content of 1.01mol%. The red line demarcates the solidus. Also, garnet-in and biotite-out is shown in green and yellow lines respectively. The abbreviation "Fs" used in pseudosections stands for feldspar.

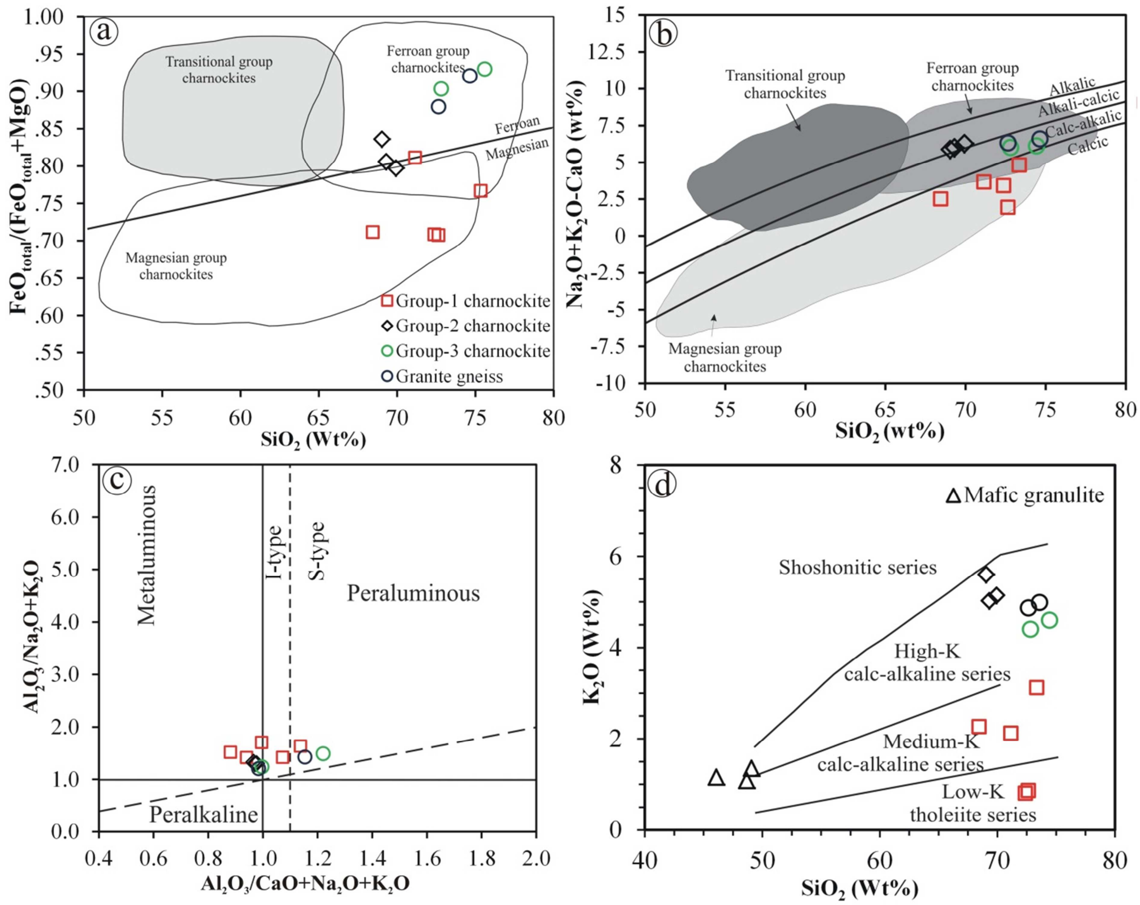

Fig. 7 Plots of charnockites and granite gneisses in (*a*) SiO_2 vs Fe-number of Frost et al. (2001); *b*, SiO_2 vs MALI of Frost et al. (2001); *c*, A/CNK vs A/NK of Shand (1943); and *d*, K_2O vs SiO_2 plot from Rickwood (1989).

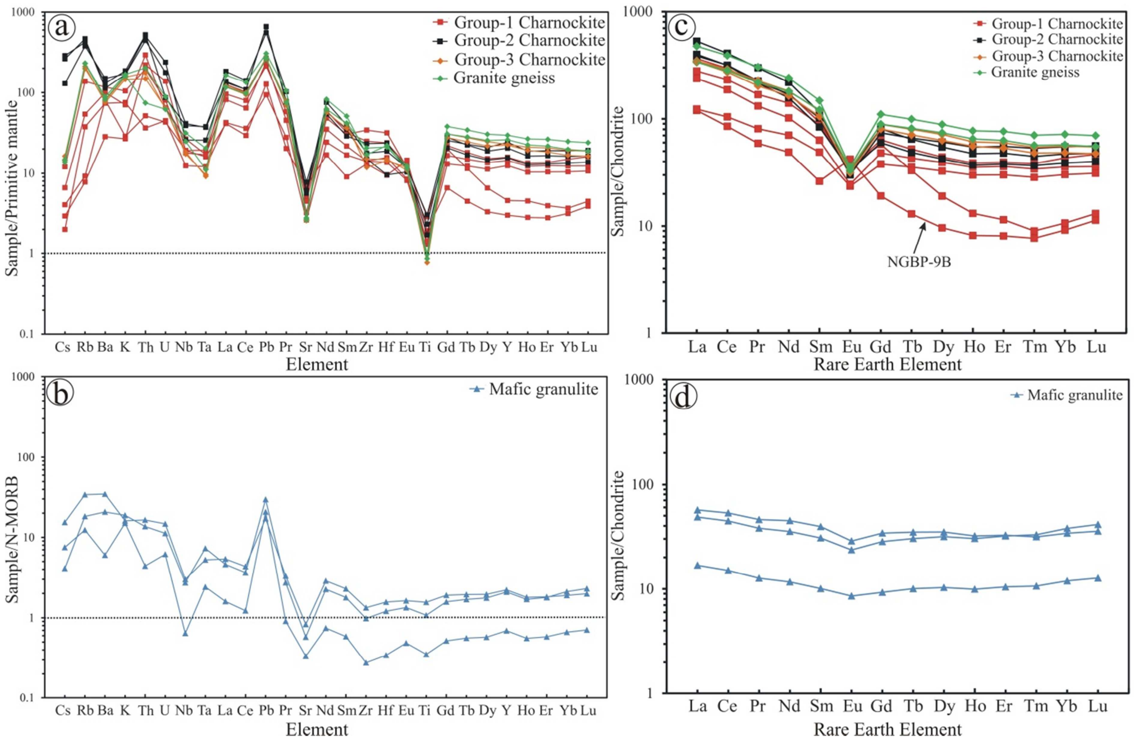

Fig. 8 Primitive mantle-normalized (*a*) and N-MORB normalized (*b*) multi-element diagrams and chondrite normalized REE patterns (*c* and *d*) in the three groups of charnockites and granite gneisses (*a, c*)**,** and mafic granulites (*b, d*). The chondrite, primitive mantle and N-MORB normalization factors are taken from Sun and McDonough (1989).

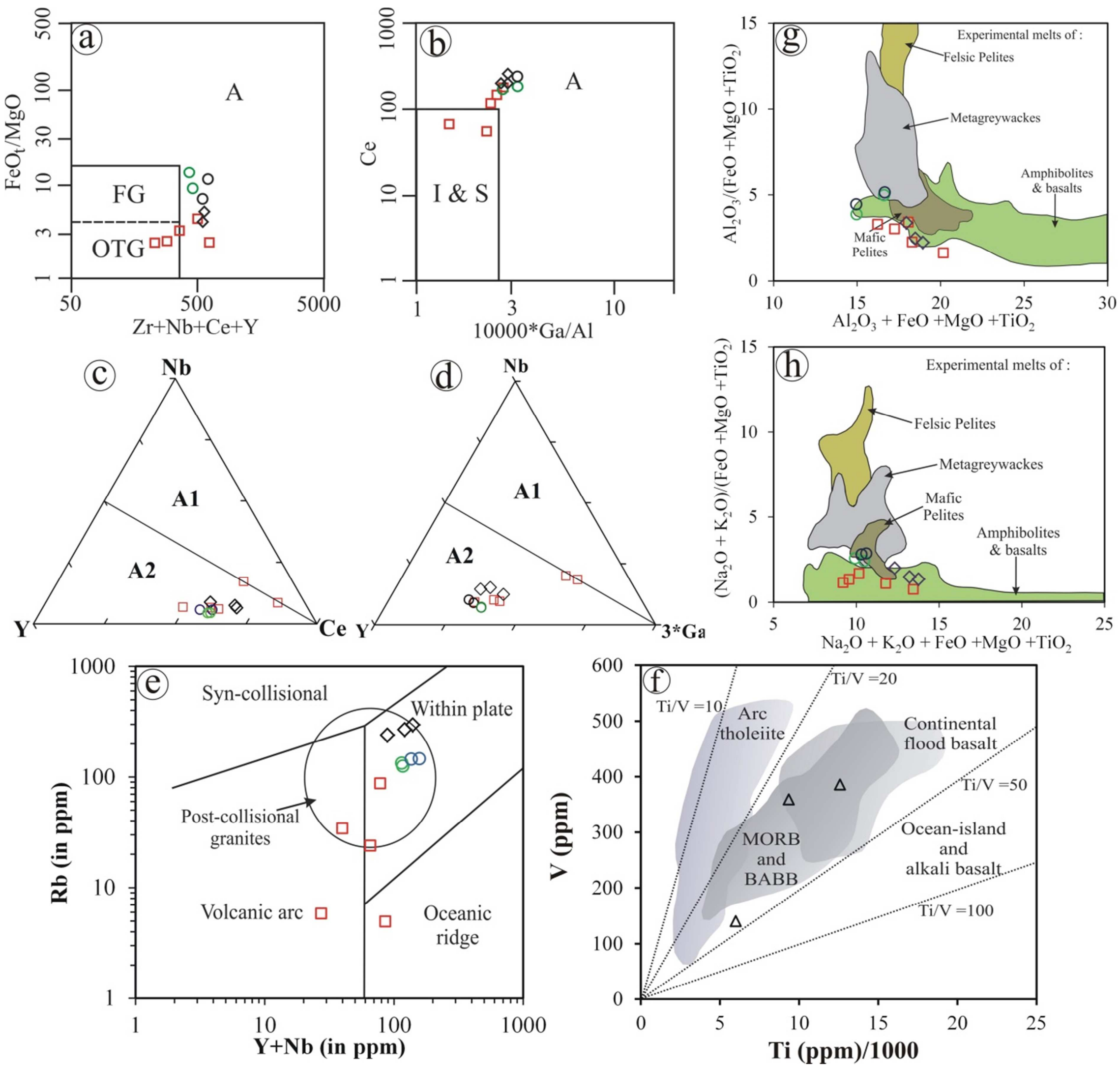

Fig. 9 Compositions of felsic and mafic lithologies plotted in different discrimination diagrams: *a*, FeO_t/MgO vs Zr+Nb+Ce+Y plot and *b*, Ce vs 10000*Ga/Al plot after Whalen et al. (1987); *c, d,* Classification of A-type granitoids (after Eby 1992) display A_2 type tectonic environments for the samples; *e*, Y + Nb vs Rb (ppm) diagram demonstrating mostly post-collision nature of the felsic rocks. Fields are after Pearce (1996); *f*, Ti (ppm)/1000 vs V(ppm) diagram of Shervais (1982) reveals continental flood basalt tectonic settings for mafic granulites; *g, h,* Plots showing compositions of the charnockite varieties, granite gneiss in comparison with compositional fields of experimental melts derived from partial melting

of felsic pelites, metagreywackes, amphibolite/metabasalt and metatonalites after Patiño Douce (1999).

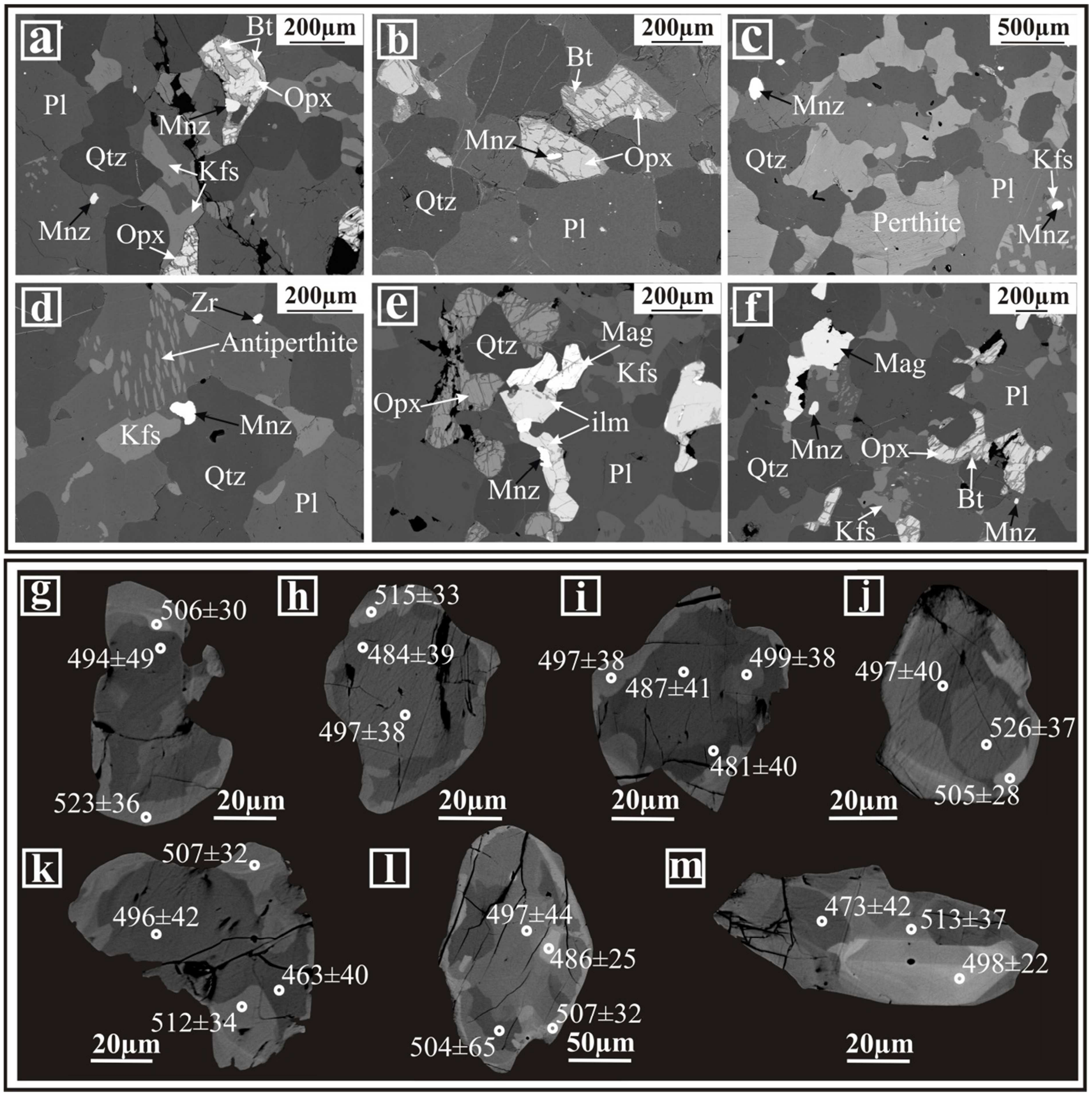

Fig. 10 BSE images showing textures of monazite in the charnockites (*a–f*). BSE images (*g-m*) demonstrate complexly zoned monazite grains. Numbers keyed to the BSE images are spot ages with their 2σ errors (in Ma). Monazite occurring (*a*) at the border and (*b*) within orthopyroxene; *c, f*, monazite occurring with K-feldspar lamellae within antiperthite; *d*,

monazite and zircon sharing grain boundaries of plagioclase, K-feldspar and quartz, respectively; *e*, monazite also at the grain boundary of ilmenite.

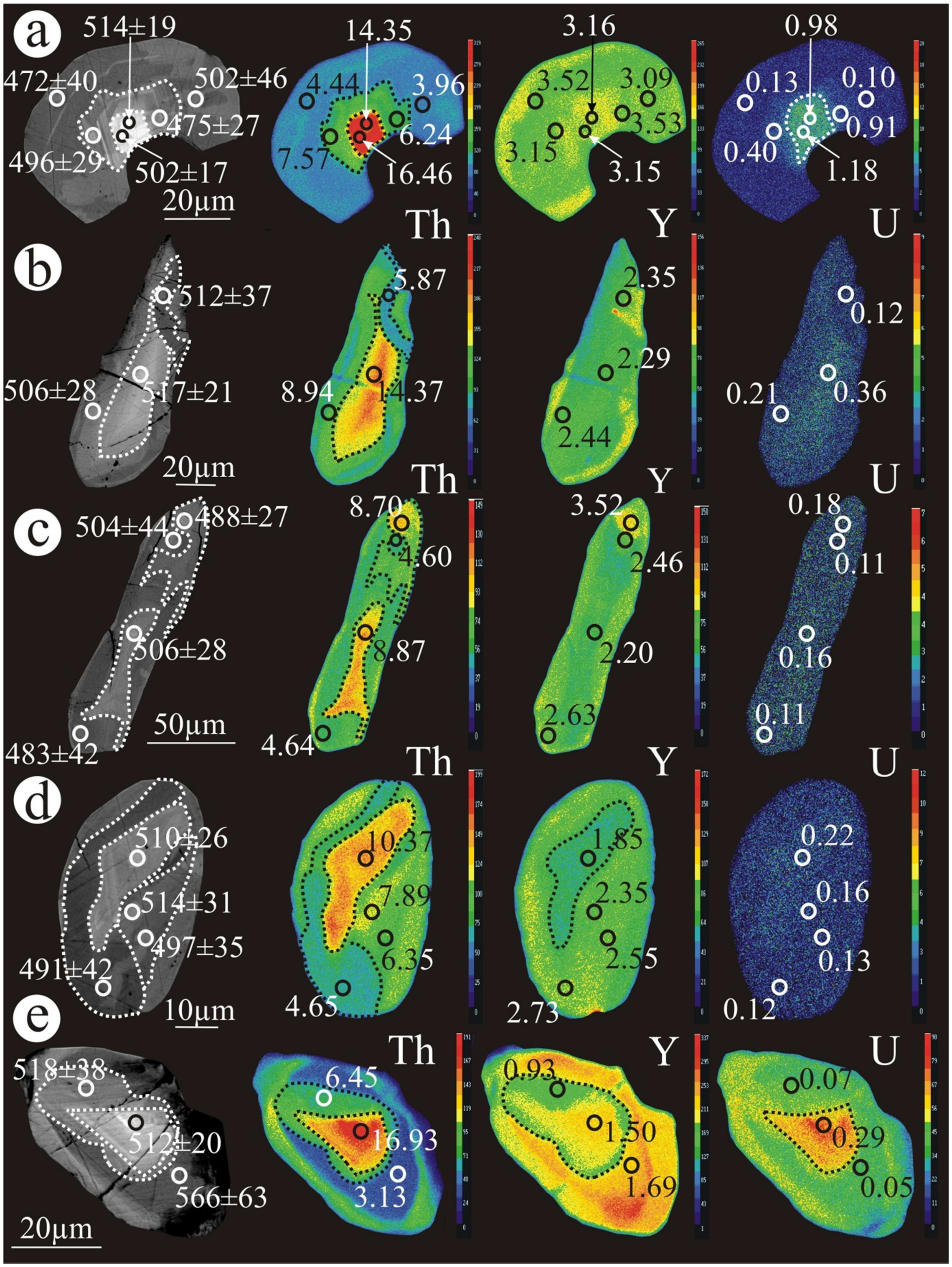

Fig. 11 BSE and X-ray images of Th, Y and U of representative monazite grains (*a*–*e*) in three charnockite samples. Spot ages with 2σ uncertainties (in Ma), and respective Th, Y and U contents (in wt.%) are shown. The compositional zones are marked by dotted lines.

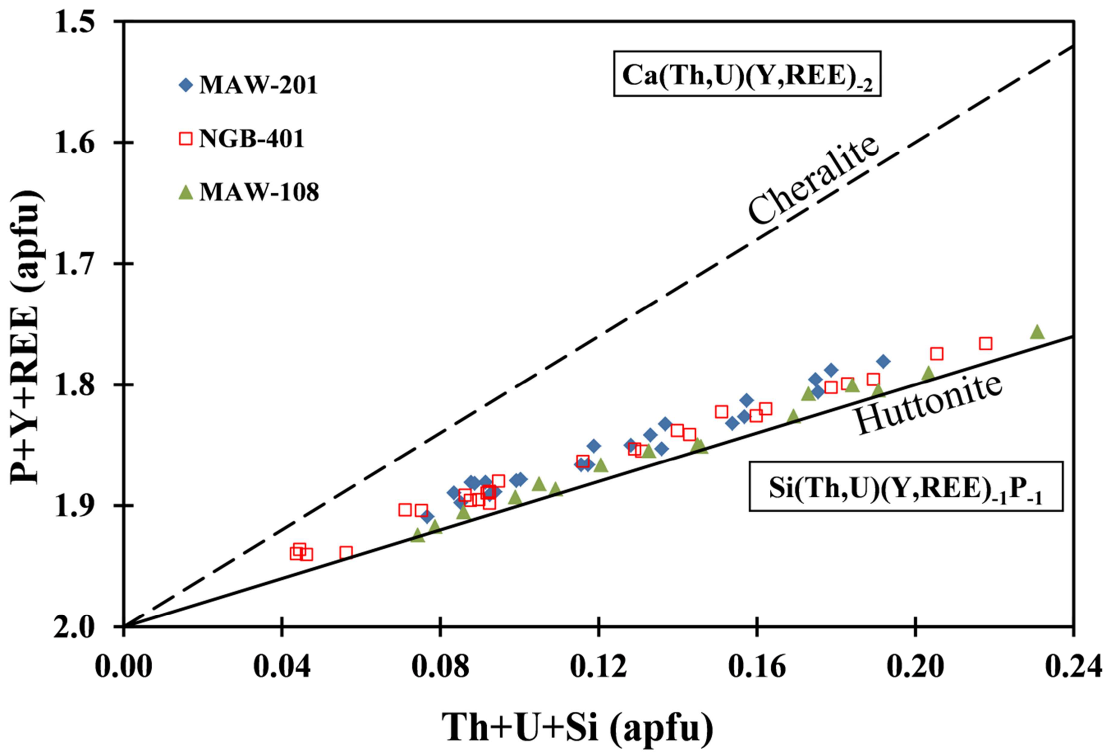

Fig. 12 Age probability plots with histograms (*a, c* and *e*), and plots showing weighted mean ages (*b, d* and *f*) of monazites from sample MAW-201 (*a* and *b*), NGB-401 (*c* and *d*) and MAW-108 (*e* and *f*). The weighted-mean age distributions and cumulative histograms are plotted using the ISOPLOT 4.15 program (Ludwig 2012).

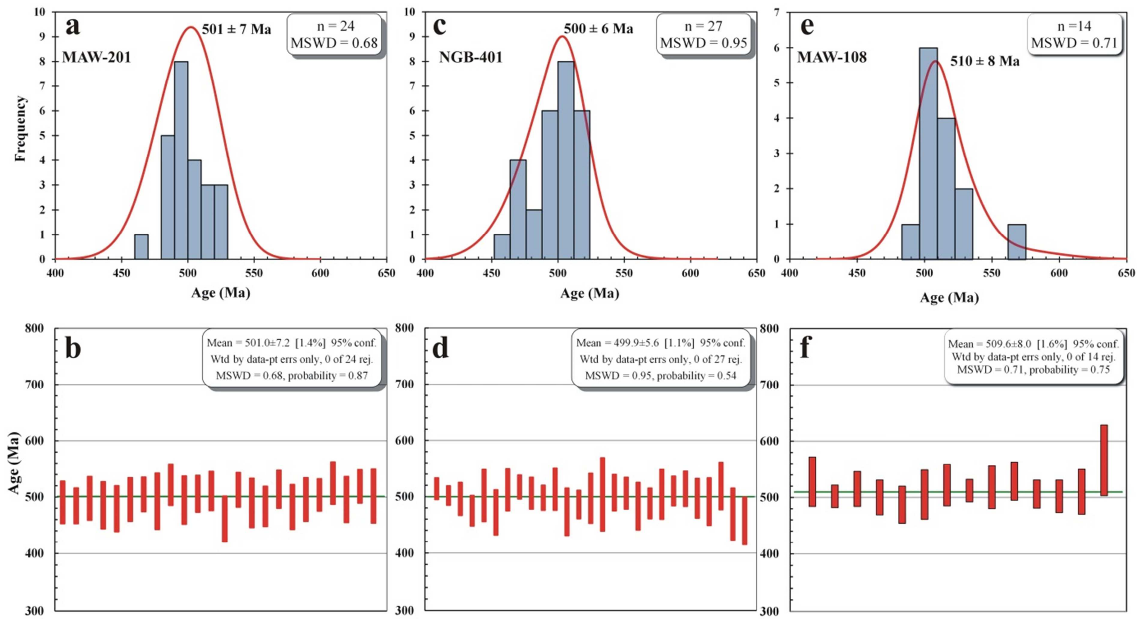

Fig. 13 Th+U+Si (apfu) vs P+Y+REE (apfu) plots of monazites in the three charnockite samples. The compositional heterogeneity is due to solid solution along the monazite-huttonite binary.

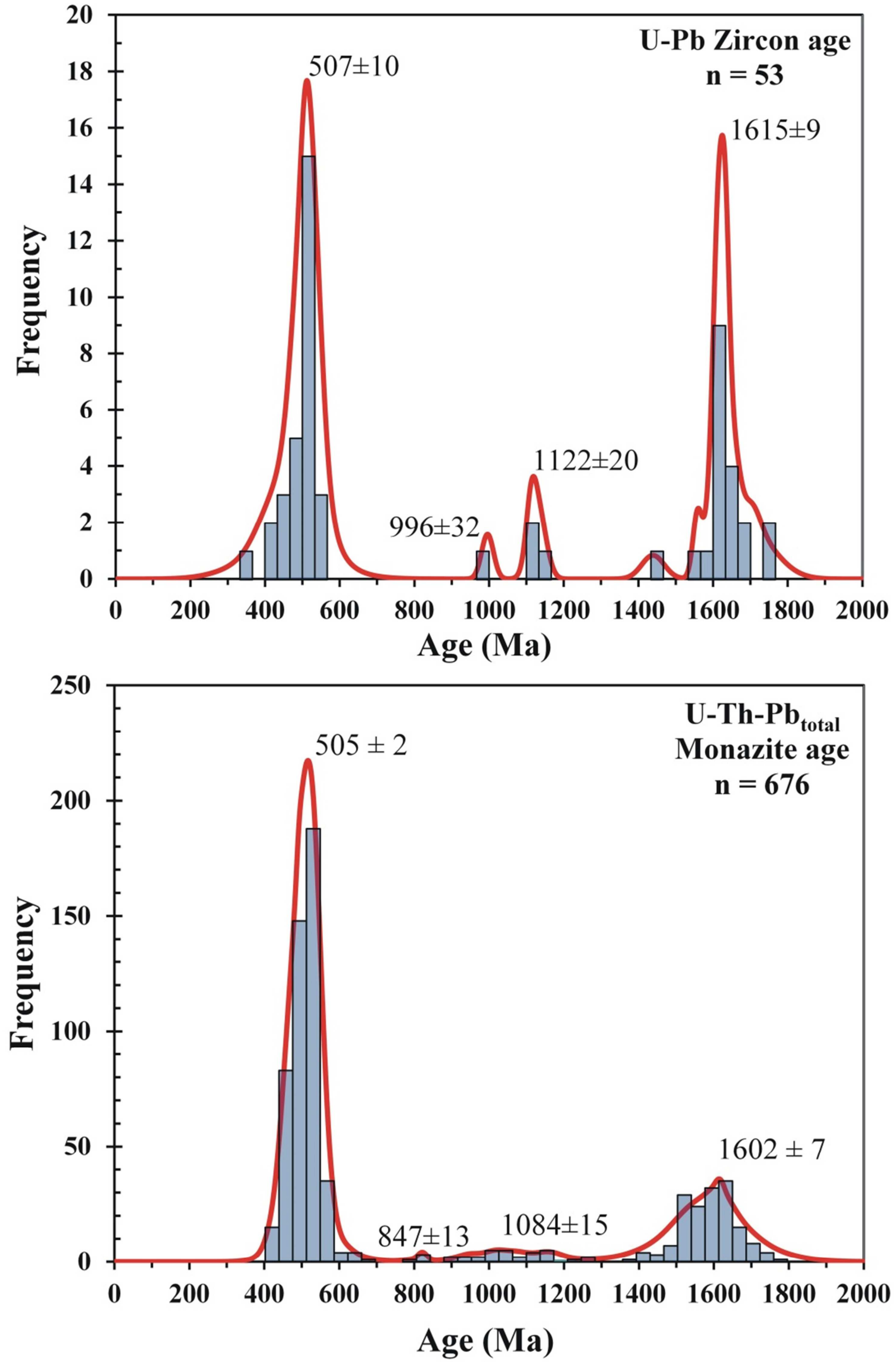

Fig. 14 Probability density plots for age determinations in SMGC: *a,* U-Pb (zircon) concordant dates (with < 2% discordance) from published data (Bidyananda and Deomurari 2007; Doley et al. 2022; Kumar et al. 2017a; 2017b; Yin et al. 2010); *b*, Monazite chemical dates with 2σ errors less than 10% from published data of Borah et al. (2019), Chatterjee et al. (2007; 2011), Dwivedi et al. (2020) and Sadiq et al. (2017).

Tables:

Table 1- Comparative results of minerals in modal percentage for different varieties of charnockites, mafic granulite and granite gneiss

Rock type	Major minerals								Accessory minerals					
	Opx	Cpx	Pl	Kfs	Qtz	Bt	Hbl	Ol	Ap	Ilm	Mag	Mnz	Zrn	Rt
Group-1 Charnockite	8-15	5-10	35-60	10-15	15-30	8-13	-	-	P	P	P	P	P	-
Group-2 Charnockite	4-9	-	15-30	38-65	20-35	5-9	1-3	-	P		P	P	P	-
Group-3 Charnockite	-	-	17-27	40-58	23-29	10-17	3-7	5-11	P	P	P	-	P	-
Mafic granulite (Pyroxene granulite)	10-25	15-30	30-38	P	~3	-	~3	-	P	P	P	-	P	P
Mafic granulite (Hornblende pyroxene granulite)	5-8	10-15	25-32	-	P	-	15-38	-	P	P	P	-	P	-
Granite gneiss	-	-	16-27	34-49	21-41	4-7	3-5	-	P	P	P	-	P	-

Table 2: Summary of thermobarometric estimation for rocks representing metamorphic assemblage and magmatic variety of charnockites from the (central) Shillong Meghalaya Gneissic Complex

		Temperature estimation (°C)					**Pressure estimation (kbar)**		
		Opx-Cpx		Opx-Bt	Ti-in Bt	Hbl-Pl	Al-in Hbl		
Rock type	Sample no.	**WB73**	**W77**	**Wu99**	**H05**	**BH90**	**S92**	**HZ86** (±3 kbar)	**H87** (± 1 kbar)
Thermobarometric estimates of rocks representing metamorphic assemblage									
M_2 assemblage (Near Peak temperature)									
Group-1 charnockites	NGB-304	813–840 **Avg** = 829±10 **n**=8	874–922 **Avg** = 900±16 **n**=8						
	NGBP-9A	781–870 **Avg**= 827±46 n=4	825–963 **Avg**= 896±72 n= 4						
	NGB-102	789–825 **Avg**= 819±19 n=3	837–892 **Avg**= 870±29 n=3						
	NGBP-9B	783–866 **Avg** = 829±27 **n**=8	828–958 **Avg** = 899±42 **n**=8						
	RM-401	790–836 **Avg** = 820±21 **n**=5	837–907 **Avg** = 883±31 **n**=5						
	Grand average	**825 ± 29**	**893 ± 45**						
Mafic granulite	*NGBP-9A	783–863 **Avg** = 811±25 **n**=8	826–951 **Avg** = 868±38 **n**=8				5.90–6.63 **Avg = 6.34±0.24 n= 8**	5.51–6.27 **Avg**= 5.98±0.25 **n**= 8	5.81–6.66 **Avg**= 6.34±0.28 **n**= 8
	*NGB-102	789–850 **Avg** = 815±31 **n**=4	835–931 **Avg** = 875±48 **n**=4			774–794 **Avg** = 786±8 **n**=8			
	*RM-401	825–852 **Avg**= 843±13 **n**=4	891–933 **Avg**= 919±19 **n**= 4			748–804 **Avg** = 772±18 **n**=8			

		Temperature estimation (°C)					Pressure estimation (kbar)		
		Opx-Cpx		Opx-Bt	Ti-in Bt	Hbl-Pl	Al-in Hbl		
Rock type	Sample no.	**WB73**	**W77**	**Wu99**	**H05**	**BH90**	**S92**	**HZ86** (±3 kbar)	**H87** (± 1 kbar)
	NGB-302					787–843 **Avg=** 804±24 **n**=8	5.39–5.82 **Avg=** 5.58±0.15 **n**=8	5.01–5.56 **Avg=** 5.17±0.14 **n**= 14	5.25–5.75 **Avg=** 5.43±0.16 n= 14
	Grand average	**821 ± 27**	**882 ± 42**			**787 ± 22**	**5.96 ± 0.44**	**5.58 ± 0.46**	**5.88 ± 0.51**
M_3 assemblage (Post Peak temperature)									
Group-1 charnockites	NGB-304			628–674 **Avg=** 649±24 **n**=4	747–766 **Avg** = 758±8 **n**=4				
	NGB-103				770-–786 **Avg** = 778±7 **n**= 4				
	Grand average			649±24	**768 ± 13**				
Granite gneiss	NGBP-21B				489–557 **Avg** = 528±25 **n**=5		5.66–6.05 **Avg =** **5.81**±0.16 **n = 5**	5.25–5.67 **Avg=** 5.41±0.18 **n=5**	5.52–5.99 **Avg=** 5.70±0.20 **n= 5**
Thermobarometric estimates for magmatic variety (group-2 and group-3) charnockites									
Group-2 charnockites	L3A					747–775 **Avg =** 756±11 n=5	5.64-6.33 **Avg =** 6.00±0.27 **n**=5	5.10–6.04 **Avg**=5.41±0.26 **n**= 10	5.35–6.41 **Avg=** 5.70±0.29 **n**=10
Group-3 charnockites	MAR-114A				672–696 **Avg** = 688±9 **n**= 6	747–797 **Avg =** 771±16 **n**=13	5.44-6.46 **Avg =** 5.71±0.34 **n**=13	5.02–6.19 **Avg=** 5.37±0.36 **n**= 13	5.26–6.57 Avg= 5.66±0.41 **n**= 13
	Grand average				**688 ± 9**	**767 ± 16**	**5.75 ± 0.32**	**5.39 ± 0.32**	**5.67 ± 0.35**

Abbreviations: **Avg.** = Average, **S.D.** = Standard deviation, **n=** no. of analyses used

WB73= Wood and Banno (1973); **W77=** Wells (1977); **Wu99=** Wu et al. (1999); **H05=** Henry et al. (2005); **BH90** = Blundy and Holland (1990); **S92=** Schmidt (1992); **HZ86=** Hammarstrom and Zen (1986); **H87=** Hollister et al. (1987)

* used in sample no. indicates analysed samples represent contact portion of group-1 charnockite and mafic granulite.

Table 3: Major element chemistry (in wt%) and trace element chemistry (in ppm) including rare earth elements (in ppm) in all varieties of charnockites, granite gneiss and mafic granulite from the (central) Shillong-Meghalaya Gneissic Complex. Chondrite-normalized values of Eu/Eu* are estimated from the equation of Taylor and McLennan (1985)

Rock type	Group-1 Charnockite					Group-2 Charnockite			Group-3 Charnockite		Granite gneiss		Mafic Granulite		
	NGBP -9B	NGB-304	NGB-103	NGBP-5	MAW-401	L3A	NGBP-19	NGBP-22	MAR-114A	MAR-103	MAR-114B	NGBP-21	NGBP-3	NGBP-9A	NGB-302
Major Oxide data (in Wt%)															
SiO_2	72.65	68.45	71.16	73.36	72.39	69.31	69.04	69.93	72.81	74.43	72.64	73.59	49.08	46.09	48.66
Al_2O_3	12.97	12.51	12.68	12.45	13.98	13.17	13.08	13.86	13.84	11.90	13.94	12.21	12.36	11.95	12.42
FeO	2.75	5.08	4.09	2.66	2.71	3.84	4.28	2.95	2.36	2.65	2.20	2.32	14.86	13.57	12.40
MnO	0.05	0.09	0.06	0.04	0.06	0.10	0.10	0.07	0.04	0.06	0.05	0.05	0.28	0.22	0.20
MgO	1.14	2.06	0.95	0.81	1.12	0.93	0.84	0.75	0.25	0.20	0.30	0.20	5.32	10.15	8.99
CaO	2.98	3.27	2.50	1.57	2.05	1.89	2.03	1.95	1.13	1.29	1.28	1.26	8.96	10.57	10.18
Na_2O	4.05	3.52	4.04	3.27	4.67	2.86	2.30	3.08	2.75	2.81	2.73	2.87	3.21	2.23	2.84
K_2O	0.87	2.27	2.12	3.12	0.81	5.02	5.60	5.14	4.40	4.60	4.87	4.99	1.35	1.16	1.09
TiO_2	0.39	0.52	0.58	0.31	0.26	0.56	0.74	0.40	0.16	0.21	0.21	0.22	1.56	2.10	1.00
P_2O_5	0.10	0.15	0.18	0.04	0.04	0.17	0.21	0.15	0.02	0.03	0.04	0.04	0.17	0.14	0.12
Total	98.25	98.48	98.80	97.63	98.37	98.26	98.22	98.60	98.03	98.18	98.50	97.75	97.15	99.69	99.29
Na_2O+ K_2O	4.92	5.79	6.16	6.39	5.48	7.88	7.90	8.22	7.15	7.41	7.60	7.86	4.56	3.39	3.93
K_2O/ Na_2O	0.21	0.64	0.53	0.95	0.17	1.76	2.43	1.67	1.60	1.64	1.78	1.74	0.42	0.52	0.38
FeO/ MgO	2.42	2.47	4.30	3.28	2.43	4.15	5.10	3.93	9.34	13.27	7.28	11.61	2.79	1.34	1.38
A/CNK	1.00	0.88	0.94	1.07	1.14	0.97	0.97	0.98	1.22	1.00	1.15	0.98	0.54	0.50	0.51
Trace element data (in ppm)															
Sc	8.37	7.39	3.89	5.61	7.12	7.54	8.53	6.21	2.15	4.51	3.41	3.36	43.29	53.06	23.28

Rock type	Group-1 Charnockite					Group-2 Charnockite			Group-3 Charnockite		Granite gneiss		Mafic Granulite		
	NGBP-9B	NGB-304	NGB-103	NGBP-5	MAW-401	L3A	NGBP-19	NGBP-22	MAR-114A	MAR-103	MAR-114B	NGBP-21	NGBP-3	NGBP-9A	NGB-302
V	11.54	20.11	18.93	12.29	7.83	20.86	22.19	17.85	6.34	7.61	6.72	7.62	358.93	385.84	140.17
Cr	21.20	35.59	25.07	11.30	22.22	19.71	18.15	16.39	10.81	8.31	11.14	11.07	84.03	195.37	57.00
Co	4.28	4.33	5.96	2.80	3.22	5.40	6.54	4.18	2.01	2.22	1.86	2.16	49.20	54.35	24.22
Ni	5.69	5.51	5.27	2.74	2.18	3.65	3.55	3.38	1.31	1.46	1.41	1.73	42.05	70.95	22.05
Ga	15.48	9.82	18.41	15.58	18.82	20.39	20.37	19.46	20.07	20.41	20.19	20.84	23.31	21.55	8.62
Ge	1.00	1.01	1.94	1.34	1.66	1.92	2.34	1.75	1.71	1.87	1.72	1.89	3.23	3.34	1.37
Rb	5.86	23.92	34.31	87.68	4.95	296.66	269.02	240.32	133.83	126.06	146.08	147.13	10.20	19.02	6.92
Sr	144.93	55.32	109.28	68.34	94.55	118.52	128.69	163.41	54.45	55.77	55.98	58.76	52.08	74.54	30.07
Y	13.68	56.72	20.84	65.55	71.95	110.55	93.27	70.59	102.28	104.02	118.47	134.70	58.45	62.06	19.37
Zr	146.69	156.81	279.54	158.52	383.84	168.40	199.12	261.47	167.66	132.41	230.33	190.77	72.57	98.63	20.41
Nb	13.69	8.85	19.02	12.74	13.69	29.45	27.82	18.41	12.36	13.05	17.67	22.49	6.36	6.97	1.50
Sn	3.04	1.39	2.89	2.09	2.72	6.87	2.51	2.2	2.7	2.67	2.01	3.2	9.5	2.57	0
Cs	0.03	0.02	0.05	0.10	0.02	2.07	2.28	1.02	0.13	0.11	0.12	0.11	0.03	0.11	0.05
Ba	563.70	515.53	697.70	814.89	198.56	793.41	906.83	1045.41	528.35	556.63	572.60	618.44	130.41	217.89	37.87
Hf	2.92	4.24	7.39	4.84	9.80	2.96	5.81	7.32	4.63	4.41	6.55	6.84	2.48	3.21	0.70
Ta	0.66	0.50	0.70	0.70	0.79	1.52	1.55	1.05	0.39	0.38	0.46	0.84	0.96	0.69	0.32
Pb	9.07	6.68	19.12	17.01	15.15	47.01	39.25	46.61	19.07	19.18	18.71	21.69	8.89	5.16	6.22
Th	4.37	3.10	24.87	16.57	18.73	37.75	44.52	42.88	12.62	14.94	6.32	17.17	1.64	1.97	0.53
U	0.90	0.94	1.36	1.69	2.90	3.71	1.82	4.99	1.35	1.33	1.30	1.87	0.53	0.69	0.29
La	28.38	29.19	86.42	56.29	66.01	91.43	125.64	94.60	80.61	82.20	79.79	112.52	11.50	13.44	3.98
Ce	52.10	63.84	180.53	114.40	141.46	193.55	249.50	192.79	166.64	177.29	172.34	238.19	27.23	32.47	9.18
Pr	5.61	7.67	20.42	12.51	15.98	21.37	28.32	20.27	19.20	21.50	20.66	28.86	3.61	4.36	1.20
Nd	22.83	32.87	80.23	47.55	65.40	78.49	102.25	73.40	76.67	84.61	84.13	111.85	16.49	20.94	5.44
Sm	4.01	7.48	14.23	9.66	13.54	15.55	17.66	12.85	16.09	18.27	18.56	22.67	4.69	6.02	1.54
Eu	2.44	1.37	2.10	1.42	1.98	1.74	1.95	1.91	1.83	1.98	1.92	2.07	1.37	1.66	0.50
Gd	3.93	7.79	11.89	9.88	13.09	15.23	16.62	12.32	16.51	18.29	18.31	22.64	5.81	7.01	1.91

Rock type	Group-1 Charnockite					Group-2 Charnockite			Group-3 Charnockite		Granite gneiss		Mafic Granulite		
	NGBP-9B	NGB-304	NGB-103	NGBP-5	MAW-401	L3A	NGBP-19	NGBP-22	MAR-114A	MAR-103	MAR-114B	NGBP-21	NGBP-3	NGBP-9A	NGB-302
Tb	0.49	1.33	1.24	1.61	1.95	2.47	2.42	1.82	2.65	2.99	3.05	3.71	1.13	1.30	0.38
Dy	2.45	8.32	4.84	10.00	11.19	15.43	13.86	10.76	15.99	18.20	18.83	22.48	8.01	8.87	2.62
Ho	0.46	1.70	0.74	2.01	2.20	3.09	2.68	2.10	3.15	3.46	3.68	4.38	1.71	1.81	0.56
Er	1.34	4.99	1.90	5.97	6.54	9.18	7.92	6.28	8.82	9.89	10.41	12.63	5.30	5.40	1.73
Tm	0.20	0.73	0.23	0.87	0.98	1.36	1.14	0.94	1.22	1.38	1.45	1.79	0.84	0.80	0.27
Yb	1.56	5.15	1.81	6.08	7.36	9.35	8.00	6.60	8.21	9.49	9.74	12.21	6.43	5.78	2.03
Lu	0.29	0.79	0.33	0.91	1.19	1.42	1.21	1.02	1.21	1.40	1.40	1.77	1.05	0.90	0.32
∑REE	125.79	172.42	406.59	278.25	347.66	458.25	577.97	436.64	417.59	449.55	442.85	595.99	94.12	109.88	31.32
K/Rb	1228.74	786.99	513.37	295.39	1349.92	140.56	172.80	177.66	273.05	302.91	276.64	281.54	1098.22	506.37	1302.47
Sr/Y	10.60	0.98	5.24	1.04	1.31	1.07	1.38	2.31	0.53	0.54	0.47	0.44	0.89	1.20	1.55
Rb/Sr	0.04	0.43	0.31	1.28	0.05	2.50	2.09	1.47	2.46	2.26	2.61	2.50	0.20	0.26	0.23
Ba/Sr	3.89	9.32	6.38	11.92	2.10	6.69	7.05	6.40	9.70	9.98	10.23	10.53	2.50	2.92	1.26
$(La/Yb)_N$	13.09	4.07	34.18	6.64	6.43	7.01	11.27	10.28	7.04	6.22	5.87	6.61	1.28	1.67	1.41
$(La/Sm)_N$	4.57	2.52	3.92	3.76	3.15	3.80	4.59	4.75	3.23	2.90	2.78	3.20	1.58	1.44	1.67
$(Gd/Yb)_N$	2.09	1.25	5.42	1.34	1.47	1.35	1.72	1.54	1.66	1.59	1.55	1.53	0.75	1.00	0.78
$(La/Lu)_N$	10.58	3.95	27.87	6.60	5.96	6.88	11.10	9.96	7.16	6.31	6.09	6.80	1.18	1.59	1.33
Eu/Eu*	1.88	0.55	0.49	0.45	0.45	0.35	0.35	0.46	0.34	0.33	0.32	0.28	0.80	0.78	0.88

Supplementary Files

This is a list of supplementary files associated with this preprint. Click to download.

- Appendix1.xlsx
- Appendix2.xlsx
- ExplanationstoSupplementaryinformation.docx
- SupplementaryFigure1.jpg